3. Results

3.1 Functional analysis of the STAT1 N-domain

3.1.1 The N-domain is required for nuclear accumulation of STAT1 following cytokine stimulation

In an attempt to understand the contribution of the STAT1 N-domain to nuclear accumulation of STAT1 we analysed the subcellular distribution and nuclear accumulation behaviour of different STAT1 mutants. The mutants were tagged with green fluorescent protein (GFP) in order to monitor the trafficking of STAT1 in living cells. The behaviour of STAT1-GFP has previously been shown to be similar to that of native STAT1. Upon IFNγ stimulation, it is activated, accumulates in the nucleus, and it is able to initiate gene expression, although with lesser efficiency than untagged STAT1 (Köster and Hauser 1999; Begitt et al., 2000, and Fig. 3.1). HeLa S3 cells were transiently transfected with wild type STAT1-GFP (WT) or a N-terminal deletion mutant, lacking the first 126 amino acids (ΔN). Twenty-four hours after transfection, the cells were stimulated for 1 h with IFNα or IFNγ. Subsequently, the cells were fixed and the nucleocytoplasmic distribution of the GFP fluorescence was evaluated (green).

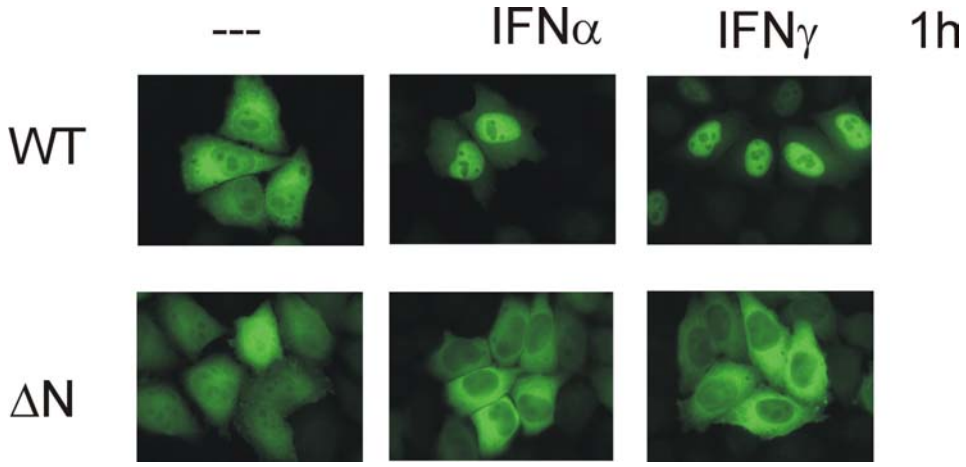

Fig. 3.1 Deletion of the N-terminal domain precludes nuclear accumulation of STAT1. HeLa S3 cells expressing STAT1-GFP wild type (WT) or the N-terminal deletion mutant ΔN (lacking amino acids 1-126) were stimulated with IFNα or IFNγ for 1 h or left untreated. GFP fluorescence was evaluated in fixed cells.

As can be seen in Fig. 3.1, the wild type STAT1 protein readily accumulated in the nuclei of HeLa S3 cells upon interferon treatment. However, the mutant protein lacking the N-domain (ΔN), did not accumulate in the nucleus following IFNα or IFNγ stimulation, confirming previous results (Strehlow and Schindler, 1998). Interestingly, also the distribution of STAT1ΔN in resting cells differed from that of the wild type. While wild type STAT1 is predominantly localised to the cytoplasm in untreated HeLa S3 cells, the N-terminal truncation mutant can be found in both the cytoplasmic and the nuclear compartment with the same intensities (Fig. 3.1, left). Moreover, the localisation of STAT1ΔN changed during the course of interferon treatment: STAT1ΔN was absent from the nucleus after a 1 h stimulation with either IFNα or IFNγ (Fig 3.1, bottom). Taken together, these observations underlined the importance of the N-domain in regulating the nucleocytoplasmic distribution of STAT1 in both untreated and interferon-stimulated cells.

3.1.2 The STAT1 N-domain does not contain an autonomous, transferable NLS

In order to examine if the isolated N-domain may provide any transport activity, the N-domain (aa 1-132) was expressed in HeLa S3 cells as a GFP fusion protein, and its distribution was compared to that of GFP. As can be seen in Fig. 3.2A, GFP alone was evenly distributed throughout the cell. Due to its small size (27 kDa) it is able to cross the nuclear pore complex (NPC, see 1.4.2) by free diffusion. Fusion of the N-domain to GFP creates a fusion protein of the size of 42 kDa, which is still small enough to pass the aqueous channel of the NPC. Any changes in the localisation of the fusion protein should therefore reflect a transport activity provided by the N-domain. However, no difference to the pancellular distribution of GFP was observed, when the fusion protein was expressed in HeLa S3 cells (N-GFP, Fig. 3.2A).

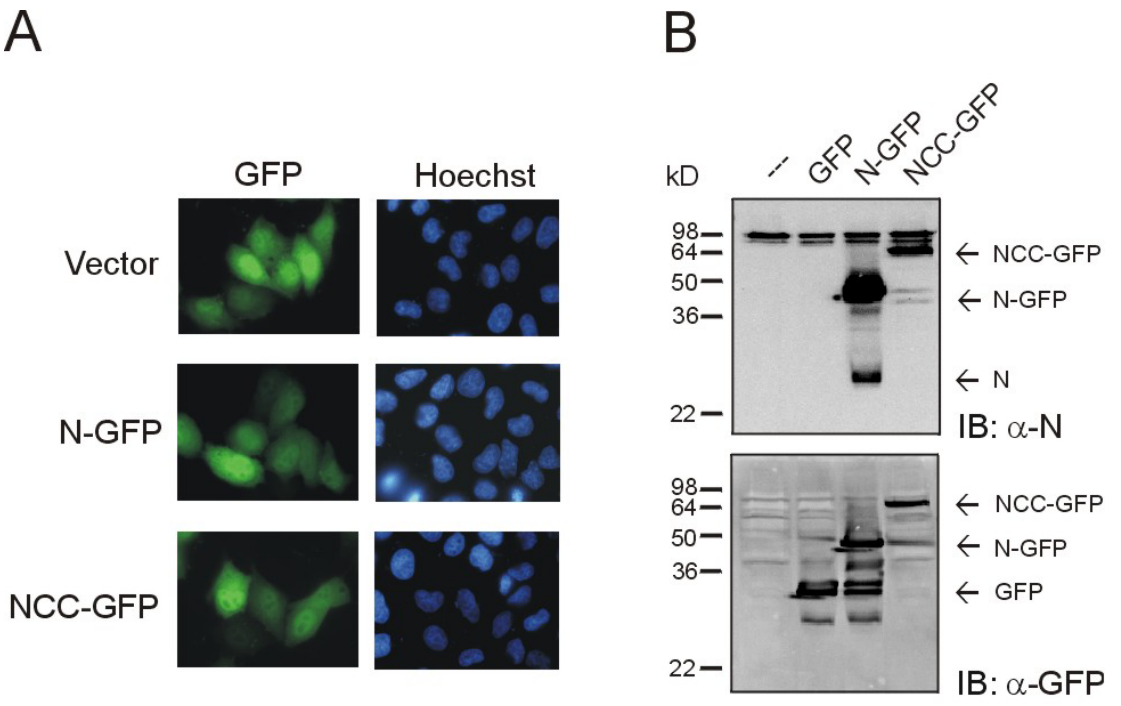

Fig. 3.2 Localisation and stability of STAT1-GFP fusion proteins in HeLa S3 cells. (A) HeLa cells were transiently transfected with expression plasmids coding for GFP (vector), the STAT1 N-domain (N-GFP) or the N-domain together with the coiled-coil domain (NCC-GFP). Twenty-four hours after transfection, the cells were fixed and the nucleocytoplasmic distribution of the GFP fluorescence was evaluated (green). To indicate the position of the nuclei the cells were stained with Hoechst 33258 (blue). (B) Western blot analysis of HeLa S3 cells expressing the same fusion proteins as in (A). Whole cell extracts were prepared and analysed with antibodies directed against the STAT1 N-domain (α-N, upper panel) or against GFP (α-GFP, lower panel). N = N-domain, CC = coiled-coil domain, NCC = N-domain and coiled-coil domain.

A recent report described a constitutive import signal in the coiled-coil domain of STAT3 (Ma et al., 2003). Since the position of the STAT1 N-domain relative to the rest of the protein is not known, also a fusion protein of the N-domain together with the adjacent coiled-coil domain (aa 1-316) was constructed. With a size of 62 kDa, NCC-GFP is at the uppermost limit for free diffusion through the nuclear pore (Görlich and Mattaj, 1996; Suntharalingam and Wente, 2003). Again a pancellular distribution of the fusion protein similar to that of free GFP was observed in HeLa S3 cells (NCC-GFP, Fig. 3.2A). To avoid misinterpretation due to the release of free GFP, the stability of the expressed proteins was checked in a Western blot analysis. As can be seen in Fig. 3.2B, indeed the N-GFP fusion construct was unstable. Free GFP was detected with an antibody against the GFP, and conversely an additional band of higher mobility showed reactivity to an antibody directed against the N-domain, indicating the release of free N-domain. The fusion protein NCC-GFP, however, was stable.

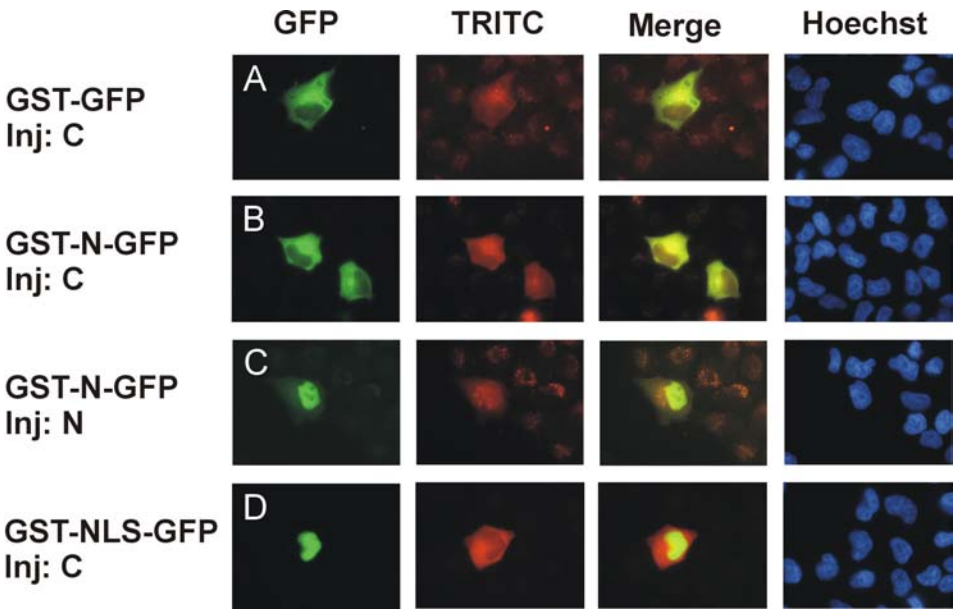

Fig. 3.3 Microinjection of the STAT1 N-domain. HeLa S3 cells grown on glass cover slips were injected with the indicated GST-GFP fusion protein. Following a 1 h incubation period the cells were fixed and stained with Hoechst 33258 (blue). The GFP signal reflects the distribution of the injected fusion protein (green). The site of injection is given by the co-injected marker protein TRITC-BSA (red). Inj: C = cytoplasmic injection, Inj: N = nuclear injection.

An alternative assay, in which the transport activity of a protein domain can be evaluated, is the microinjection of the recombinant protein as a fusion to GST-GFP. The GST-GFP fusion protein alone is unable to leave the injected compartment by free diffusion through the NPC (Fig. 3.3A), presumably due to its large size (60 kDa). Any observed difference in localisation, thus, provides evidence for a transport activity, supplied by the domain under investigation that was incorporated into the fusion protein. The assay has the advantage that the movement of the fusion protein from the injected compartment can directly be monitored by the GFP signal. For this purpose, the STAT1 N-domain (aa 1-131) was expressed as a GST-GFP fusion protein and purified from bacteria (see 2.2.14). The stability of the purified fusion protein was verified on a Coomassie-stained gel prior to injection (data not shown). HeLa S3 cells were injected either in the cytoplasmic or the nuclear compartment. Following a one hour incubation to allow transport to proceed, the cells were fixed and the subcellular distribution of the fusion proteins was analysed. TRITC-BSA was co-injected to highlight the injected compartment. As can be seen in Fig. 3.3B and C, the N-domain did not promote any transport across the nuclear envelope, neither when injected in the cytoplasm, nor following injection in the nucleus, thus ruling out an import as well as an export activity in the isolated N-domain. As a positive control a GST-GFP fusion protein

containing a classical NLS, derived from the SV40 T antigen, was used (Meyer et al., 2003). The GST-NLS-GFP fusion protein readily accumulated in the nucleus of HeLa S3 cells when injected into the cytoplasm (Fig. 3.3 D).

In an additional approach, the N-domain of STAT1 was analysed for the presence of NLS-like sequences (see 1.4.2) in the full length protein context. There are two clusters of positively charged residues on the surface of the STAT1 N-domain ([H^{81}, R^{84}, K^{85}, R^{88}]and [K^{110}, E^{111}, R^{113}, K^{114}]) that resemble monopartite NLSs (Dingwall et al., 1982), and may represent binding sites to transport receptors of the importin-α family. To assess their role in nuclear import of STAT1, single or multiple alanine substitutions were introduced in the coding sequence of STAT1-GFP, and the mutant proteins were expressed in HeLa S3 cells and analysed for their import behaviour. The results of this analysis are summarised in Fig. 3.4.

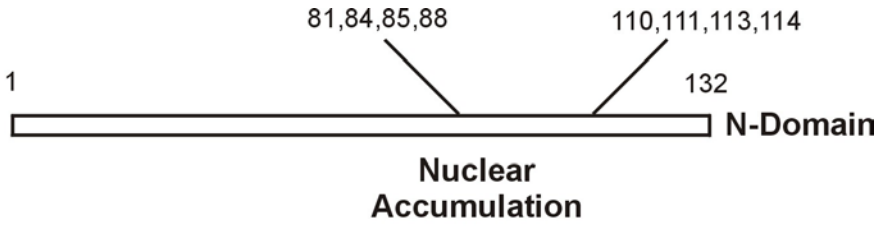

	Nuclear Accumulation
D11/S12/K13/L15	Yes
R31A	No
R70A	Yes
H81/R84/K85/R88A	Yes
K110/E111/R113/K114A	Yes

Fig. 3.4 Mutational analysis of positively charged amino acids in the STAT1 N-domain. The indicated mutants were constructed as STAT1-GFP fusion proteins and analysed for their nuclear accumulation behaviour following IFNγ stimulation in HeLa S3 cells.

As can be seen in Fig. 3.5, even the substitution of multiple charged surface residues ([H^{81}, R^{84}, K^{85}, R^{88}] and [K^{110}, E^{111}, R^{113}, K^{114}]) in the N-domain to alanine did not affect nuclear import of STAT1-GFP in HeLa S3 cells (Fig. 3.5A). Nuclear accumulation of the mutants was also observed in STAT1-deficient U3A cells, thus ruling out a contribution of heterodimerisation with endogenous wild type STAT1 (Fig. 3.5 B). The only charged residue that abolished nuclear import function upon substitution to alanine (R^{31}A) is not surface exposed and its role in maintaining the structural integrity of the N-domain will be analysed below. Taken together, the results of the localisation studies and of the microinjections showed that the isolated N-domain is devoid of transport activity. Moreover, the mutagenesis

analysis also provided no evidence for the presence of a classical, transferable NLS, indicating a rather unconventional nuclear targeting function of the STAT1 N-domain, which has to be considered in the full length protein context.

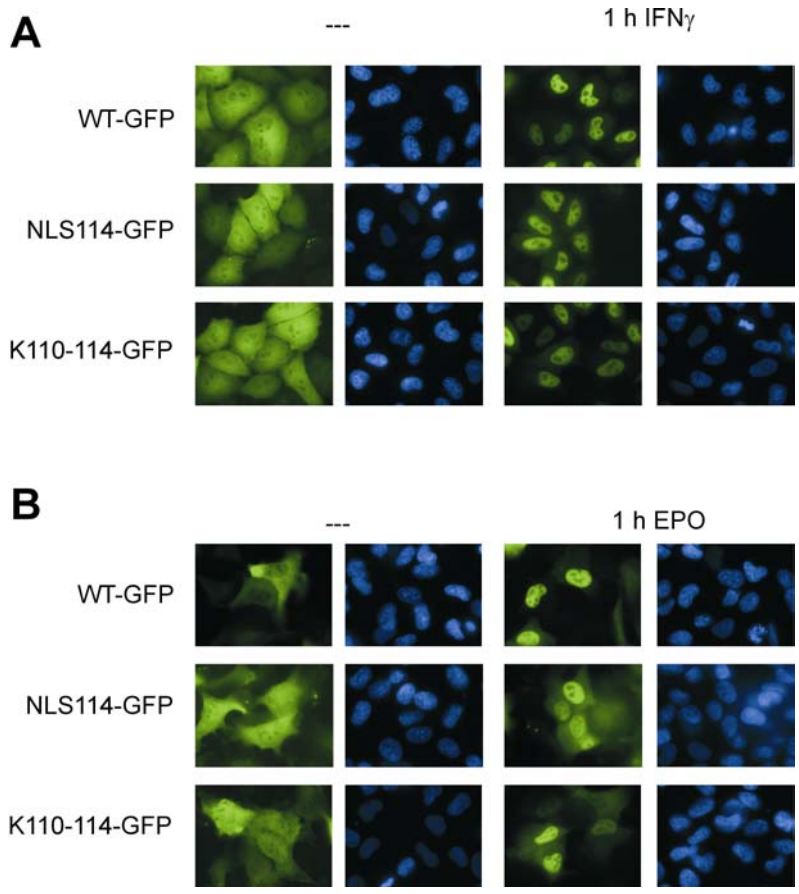

Fig. 3.5 Mutational analysis of putative NLSs in the STAT1 N-domain. (A) HeLa S3 cells transiently expressing STAT1-GFP wild type or mutants were stimulated with IFNγ for 1 h or left untreated. The NLS114 mutant contains the following alanine substitutions: $H^{81}A$, $R^{84}A$, $K^{85}A$, $R^{88}A$, whereas the K110-114 mutant had alanine substitutions in position K^{110}, E^{111}, R^{113}, K^{114}. GFP fluorescence was detected in fixed cells. The nuclei were stained with Hoechst 33258 (blue). (B) Analysis of the same STAT1-GFP fusion proteins as in (A) in STAT1-deficient U3A cells. The U3A cells were co-transfected with the human EPO receptor for enhanced STAT1 activation, following a 1 h EPO treatment.

3.1.3 The N-domain is required for STAT1 binding to importin-α5

The results of the above mutational analysis underlined the essential role of the N-domain in STAT1 nuclear accumulation. Yet, they cannot distinguish between a nuclear import defect or loss of nuclear retention (see 1.4.2), since both processes, nuclear import of STAT1 and its

retention in the nucleus, contribute to the built-up of nuclear accumulation (Meyer et al., 2003). During the course of this study, specific binding of STAT1 to the nuclear import receptor importin-α5 has been reported and the residues required for this interaction have been mapped to the DNA binding domain (aa 407-413, McBride et al., 2002; Meyer et al., 2002a). An intriguing hypothesis is that the N-domain may be required for binding of STAT1 to importin-α5 in addition to the dsNLS in the DNA binding domain. To test this hypothesis, binding of wild type STAT1 (WT) and of the N-terminal deletion mutant (ΔN) to recombinant importin-α5 was analysed. STAT1-deficient U3A cells were transfected with plasmids coding for STAT1 wild type or STAT1ΔN. Following 30 min stimulation with IFNγ, the cells were lysed and incubated for 2 h with recombinant importin-α5 (see 2.2.15). Subsequently, importin-α5 was precipitated and bound STAT1 was detected in a Western blot analysis. Expectedly, as can be seen in Fig. 3.6A, the wild type STAT1 protein did bind to importin-α5. STAT1ΔN, however, could not be co-precipitated with importin-α5, confirming the assumption that the N-domain is also required for binding of STAT1 to the nuclear import receptor. In conclusion, the nuclear accumulation phenotype of STAT1ΔN can thus be attributed to defective nuclear import, rather than to impaired retention in the nucleus.

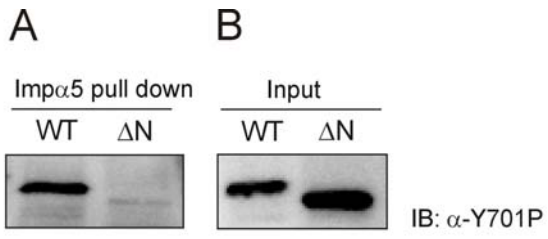

Fig. 3.6 Binding of STAT1 to importin-α5 relies on the presence of the N-domain. U3A cells were transiently transfected with the indicated STAT1 variants. Twenty-four hours after transfection, the cells were stimulated for 30 min with IFNγ. Whole cell lysates were prepared, and normalised for similar amounts of phosphorylated STAT1 (B, input), and subsequently they were used for co-precipitation with recombinant, Strep-tagged importin-α5 (A). Following repeated washing, bound STAT1 was detected in a Western blot with an anti-phosphotyrosine STAT1 antibody (α-Y701P).

3.1.4 Multiple mutations within the N-domain preclude STAT1 nuclear accumulation

We demonstrated above that the N-domain is required for binding of STAT1 to the nuclear import receptor importin-α5. However, no classical NLS could be identified in the N-domain of STAT1, and mutation of positively-charged surface residues was without consequences on the nuclear accumulation behaviour of the transcription factor (Figs. 3.4 and 3.5). In order to

narrow down the region(s) of the N-domain required for nuclear import of tyrosine-phosphorylated STAT1, a series of deletion mutants was constructed (Fig. 3.7). The mutant proteins were transiently expressed in HeLa S3 cells. Twenty-four hours after transfection, the cells were treated for 30 min with IFNγ, and the accumulation behaviour of the mutant proteins was compared to that of the wild type. Surprisingly, none of the deletion mutants retained the ability to accumulate in the nucleus of HeLa S3 cells following interferon treatment. Already deletion of the first six N-terminal residues abolished the nuclear accumulation function of the protein (Fig. 3.7 and Fig. 3.8, Δ6).

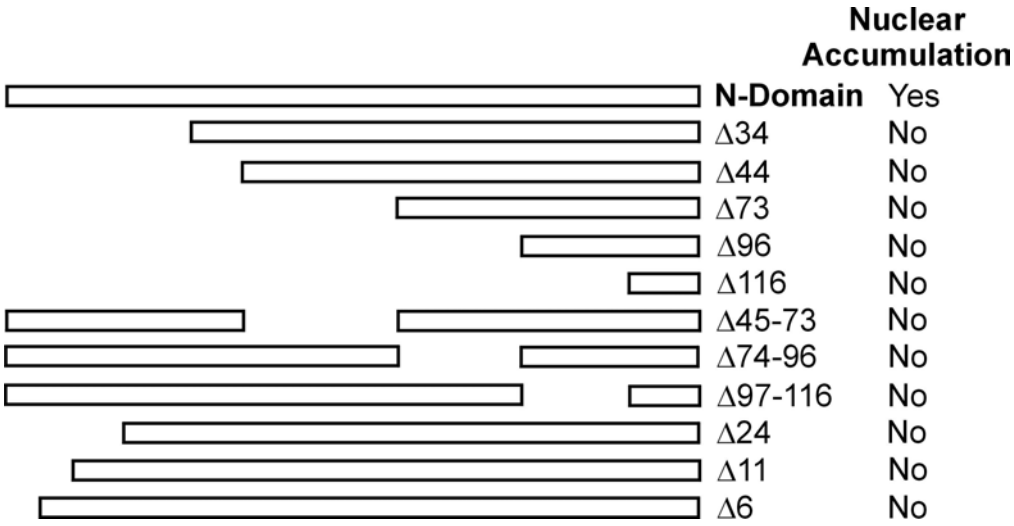

Fig. 3.7 N-terminal deletion mutants. The indicated N-terminal deletion mutants were constructed as STAT1-GFP fusion proteins and analysed for their nuclear accumulation behaviour following cytokine treatment in HeLa S3 cells.

The crystal structure of the STAT N-domain (Fig 1.3) reveals that the first α-helix (α1) contributes to the structural integrity of the whole N-domain. The residue Trp^4 is part of a buried invariant salt bridge network (W^4, R^{31}, E^{39}, E^{112}, Vinkemeier et al., 1998) that stabilises the ring-shaped element (see 1.4.1). Thus, we examined whether mutation of other residues that participate in the ring-structure also impairs nuclear accumulation. As shown in Fig. 3.8, this was indeed the case. Mutation of residues Arg^{31} and Glu^{112}, which form an ion pair, tethering the ring-shaped element together, abolished nuclear accumulation. The mutants ($R^{31}A$, $E^{112}A$) did not accumulate in the nucleus of HeLa S3 cells following IFNγ treatment. Contrary, mutation of the neighbouring Glu^{111} that according to the crystal structure has no role in N-domain architecture had no effect on the nuclear accumulation behaviour. The mutant protein ($E^{111}A$) did accumulate in the nucleus as was the case for wild type STAT1

(Fig. 3.8). Mutation of Trp^{37}, which is not part of the ring-element but nevertheless has been demonstrated to be structurally important (Vinkemeier et al., 1996, Chen et al, 2003), also resulted in a nuclear accumulation defect (Fig. 3.8, $W^{37}A$). These results strongly suggested that the observed defects in nuclear accumulation result from the compromised structural integrity of the N-domain, rather than from the contribution of single residues to the binding of importin-α5.

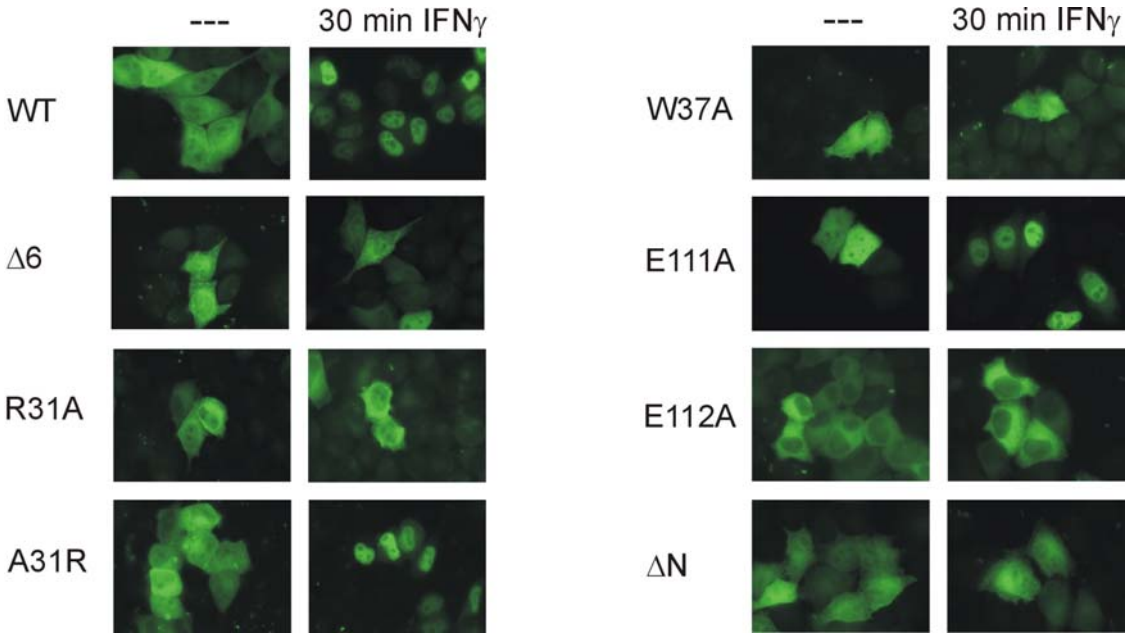

Fig. 3.8 Nuclear accumulation behaviour of wild type STAT1-GFP and N-terminal mutants. HeLa S3 cells expressing STAT1-GFP wild type or the indicated mutants were stimulated with IFNγ for 30 min or left untreated. GFP fluorescence was evaluated in fixed cells. Mutation of Arg^{31} precludes nuclear accumulation of STAT1. The revertant $A^{31}R$ could restore nuclear import function. However, even subtle sterical perturbations of the N-domain architecture ($R^{31}K$) affected STAT1 nuclear accumulation.

3.1.5 N-terminal mutants of STAT1 display impaired dephosphorylation and protein degradation

The N-domain has also been implicated in the dephosphorylation of the STAT proteins, and the conserved residue Arg^{31} has been suggested to be crucial for phosphatase recruitment (Shuai et al., 1996). Since dephosphorylation of STATs predominantly occurs in the nucleus (Haspel and Darnell, 1999; ten Hoeve et al., 2002), the observed nuclear translocation defect of STAT1ΔN and the $R^{31}A$ mutant may provide a simple explanation of the observed hyperphosphorylation phenotype (see 1.4.2). Due to their import defect, the mutants have no

access to the nuclear phosphatase and remain phosphorylated. To test this model, we also analysed the dephosphorylation kinetics of the other mutants displaying a nuclear accumulation defect (Δ6, $W^{37}A$, $E^{112}A$). Tyrosine dephosphorylation was analysed in transiently reconstituted U3A cells. The cells were first stimulated with IFNγ to induce tyrosine phosphorylation of the STAT1 variants, before adding the kinase inhibitor staurosporine to the cells for the times indicated (Fig. 3.9). Staurosporine treatment allows the monitoring of dephosphorylation in the absence of ongoing kinase activity. As can be seen in Fig. 3.9, the phosphorylation of STAT1 wild type disappeared over a period of 90 min following IFNγ stimulation. Addition of staurosporine led to a drastic reduction of the phosphorylation signal already after 30 min. As has been reported earlier (Shuai et al., 1996), removal of the N-domain (residues 1-126) created a stable molecule that strongly resisted tyrosine dephosphorylation (Fig. 3.9), supporting the role of the N-domain in dephosphorylation of STAT1. Remarkably, despite a low level of expression, all of the N-domain mutants that displayed defective nuclear accumulation (Δ6, $R^{31}A$, $W^{37}A$, $E^{112}A$) also displayed a tyrosine dephosphorylation defect, whereas the mutant $E^{111}A$ was again indistinguishable from the wild type (Fig. 3.9).

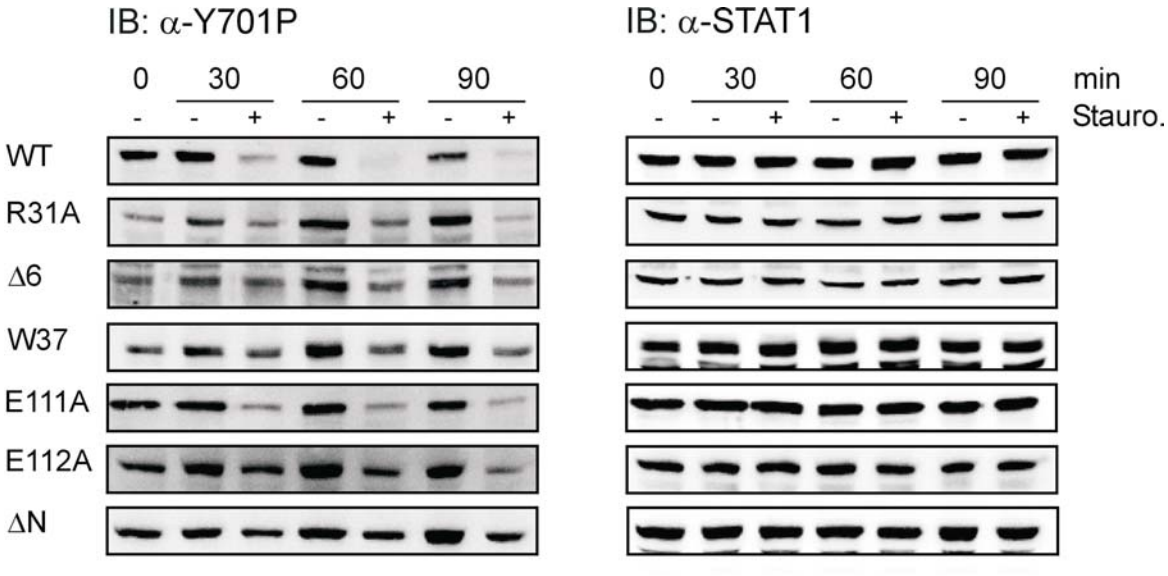

Fig. 3.9 Time-course of STAT1 tyrosine dephosphorylation in transiently reconstituted U3A cells. Cells were stimulated with IFNγ for 30 min (t=0). After the removal of IFN the cells were treated without or with the kinase inhibitor staurosporine for the indicated amount of time. Shown are Western blot results with an anti-phosphotyrosine STAT1 antibody (α-Y701P, left panel) and the reprobing with a STAT1 antibody (α-STAT1, right panel).

Mutation of arginine 31 to alanine has been reported to destabilise the STAT1 protein (Shuai et al., 1996). We therefore also analysed the expression and stability of the other mutants displaying a nuclear accumulation and dephosphorylation phenotype (Δ6, $W^{37}A$, and $E^{112}A$) in transiently reconstituted U3A cells. As was seen before (Shuai et al., 1996), replacement of the arginine residue 31 with alanine reduced the expression level of the STAT1 mutant, as indicated by the poor reactivity of whole cell extracts with antibodies directed against the N or C terminus of STAT1 (Fig. 3.10). A weak expression in U3A cells was also observed for STAT1Δ6, $W^{37}A$, and $E^{112}A$. Of note, some of the mutants were also partially degraded to STAT1ΔN, as judged by their mobility on the SDS-PAGE and the inability to detect them in a Western blot with an antibody directed against the N-domain (Fig. 3.10, upper panel). Again, mutation of the surface residue E^{111}, which according to the crystal structure has no role in maintaining the N-domain structure, did not affect the stability or expression level of the mutant protein ($E^{111}A$).

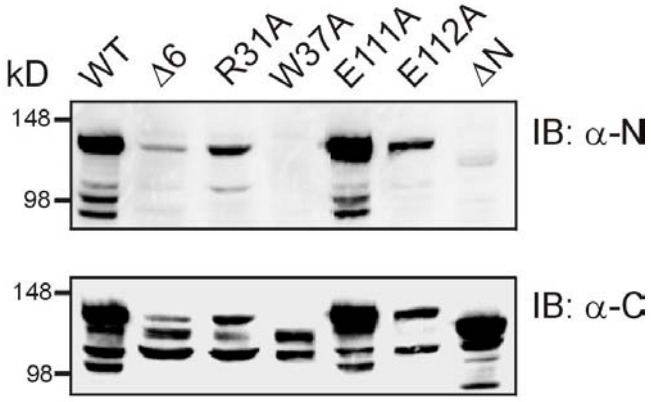

Fig. 3.10 Stability of N-terminal mutants of STAT1. Western blot with antibodies against the STAT1 N (top) or C terminus (bottom), respectively. Equal numbers of U3A cells were transiently transfected with an identical amount of cDNA encoding variant STAT1-GFP proteins. After 48 h whole cell extracts were prepared and immunoblotted. Molecular weight standards (kD) are indicated on the left.

In summary, our results revealed that mutations of residues, which according to the crystal structure stabilise the fold of the STAT1 N-domain, all result in an identical phenotype, which entails reduced expression, N-terminal degradation, defective nuclear accumulation, and impaired tyrosine dephosphorylation. We therefore concluded that functional defects formerly attributed to specific residues such as Arg^{31} may rather be caused by an unfolding of the N-domain with unspecific consequences.

Further experiments were performed to investigate the stability of the $Arg^{31}Ala$ mutant of STAT1. The isolated N-domain (residues 1-129) was expressed in bacteria as a fusion protein with either a Strep-tag or the GST-domain linked to its C terminus (see 2.2.14). Fusion proteins with the wild type N-domain were expressed well as soluble proteins (Fig. 3.11). Contrary, the Strep-tagged $Arg^{31}Ala$ mutant was not detectable by Coomassie blue staining or Western blot analysis of bacterial lysates, and the respective GST-fusion protein was insoluble (Fig. 3.11). These results strongly suggested that the native fold of the N-domain was corrupted by the mutation of arginine 31 to alanine.

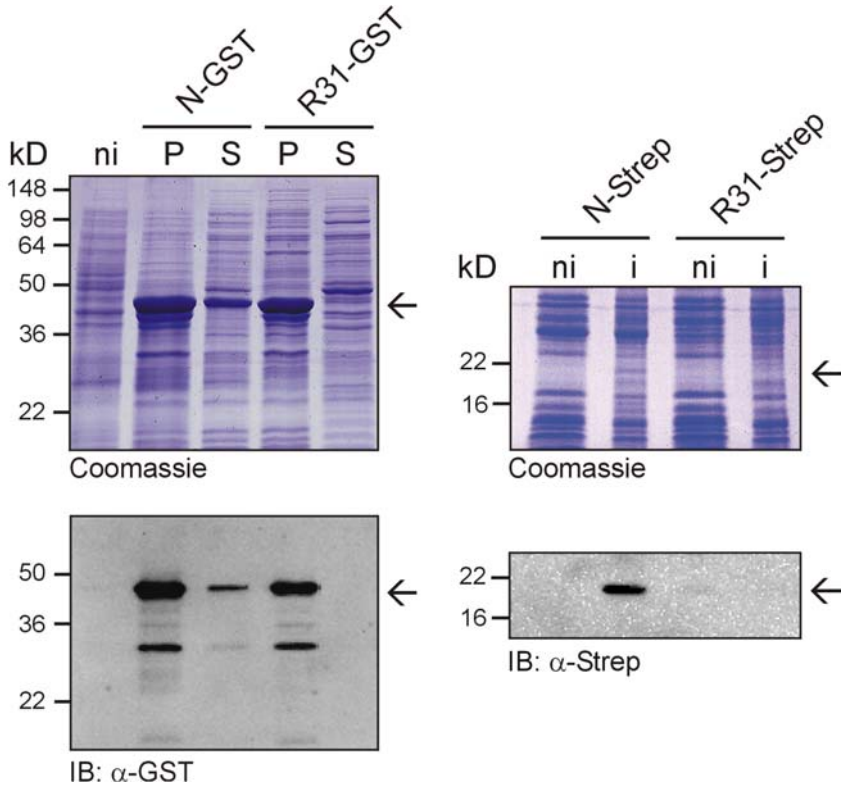

Fig. 3.11 Bacterial expression of C-terminal fusion proteins of the wild type or $R^{31}A$ mutant STAT1 N-domain with GST or Strep-tag. Shown are Coomassie blue-stained gels (top panels) and Western blot results (bottom panels). Antibodies directed against GST- or Strep-tag were reacted with 1% or 2%, respectively, of the input shown in the top panels. Whole cell lysates were prepared before (ni) or after induction (i) of recombinant protein synthesis. Alternatively, soluble (S) and insoluble (P) fractions generated by 3 freeze/thaw cycles of induced bacteria with subsequent centrifugation are shown. Molecular weight standards (kD) are indicated on the left margin, arrows denote the position of the N-domain fusion proteins.

3.1.6 Stabilisation of the $R^{31}A$ mutant does not rescue its functional defects

Of note, in mammalian cells problems with stability and solubility of the full length $R^{31}A$ mutant can be overcome by fusing GST to the STAT1 amino terminus (Shuai et al., 1996). The stabilised version of the $R^{31}A$ mutant has been used in several studies that investigated the role of STAT dephosphorylation and also of STAT1 methylation (Shuai et al., 1996; Mowen et al., 2001). The nuclear accumulation behaviour of the mutant protein, however, was not analysed in these studies. Given the nuclear translocation defect we uncovered, we were wondering if the functional defects observed upon mutation of $R^{31}A$ were rescued by the fusion to GST. As was reported by Shuai and co-workers (1996), expression and DNA binding of the STAT1-$R^{31}A$ GST-fusion protein were similar to the wild type, but the mutant retained the dephosphorylation defect (Fig. 3.12).

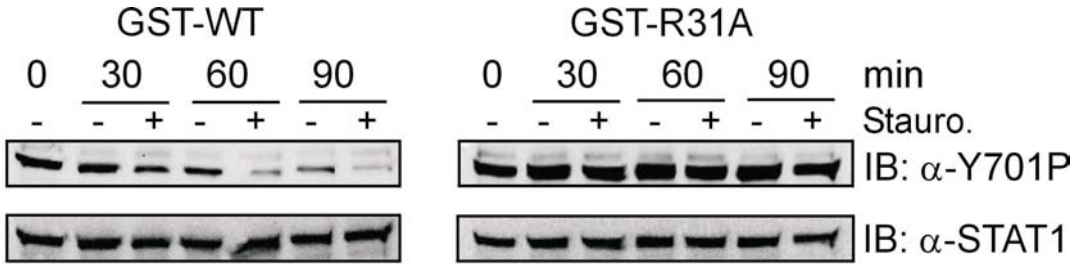

Fig. 3.12 Tyrosine dephosphorylation of wild type and $R^{31}A$ mutant of STAT1-GFP fused to the C terminus of GST. The proteins were expressed in U3A cells. Following a 30 min IFNγ pulse, the cells were either treated with the kinase inhibitor staurosporine for the indicated times or left untreated. Whole cell extracts were analysed with antibodies directed against tyrosine-phosphorylated STAT1 (α-Y701P), and subsequently with a STAT1-specific antibody (α-STAT1).

Next, we examined the nuclear accumulation behaviour of the GST-STAT1 fusion proteins (Fig. 3.13). The GST fusion of wild type STAT1 readily entered the nucleus in response to IFNγ. In order to induce nuclear accumulation after stimulation with IFNα, it was necessary to increase the number of functional IFNα receptors by co-transfection of cells with the tyrosine kinase Tyk2 and the IFNα receptor chain 1 (Ragimbeau et al., 2003). Strikingly, the $Arg^{31}Ala$ mutant had retained also the nuclear import deficiency as a GST fusion protein, as no nuclear accumulation of the heavily phosphorylated protein occurred after stimulation with IFNα or IFNγ (Fig. 3.13). Even the co-expression of the kinase c-Eyk, which has been shown to directly phosphorylate STAT1 in a receptor-independent way (Zong et al., 1996), did not induce nuclear accumulation of the $Arg^{31}Ala$ mutant.

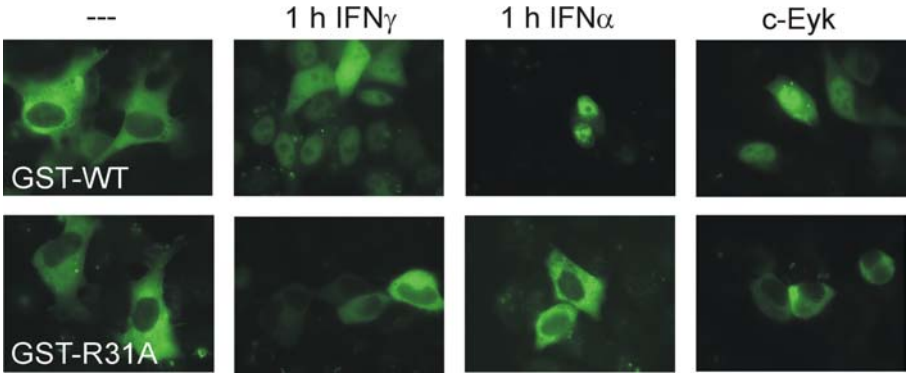

Fig. 3.13 Stabilisation of $R^{31}A$ mutant does not rescue the nuclear accumulation defect. HeLa S3 cells transiently expressing STAT1-GFP fused to the C terminus of GST were left untreated or stimulated with IFNα or -γ for 60 min. GST-STAT1 was detected in fixed cells by GFP fluorescence. IFNα stimulation was performed in HeLa cells that additionally co-expressed Tyk2 and IFNα receptor 1.

We concluded from the above experiments that mutation of Arg^{31} caused unfolding of the N-domain three-dimensional structure with unspecific functional consequences. Importantly, the breaking up of the physiological tertiary structure was not remedied by the fusion of STAT1 with GST. Fusion of STAT1-$R^{31}A$ to GST neither remedied defective dephosphorylation nor restored nuclear import. These results circumstantiate the requirement of a structurally intact N-domain for cytokine-inducible nuclear import of STAT1.

3.1.7 The $R^{31}A$ mutant does not promote reporter gene transcription in STAT1-deficient cells

The $R^{31}A$ mutant has also been used as a genetic model in the study of STAT1 methylation. It was postulated that introducing an uncharged side chain by the alanine mutation might mimic the attenuated charge effects of the methylated guanidino group of Arg^{31} (Mowen et al., 2001). Remarkably, the $R^{31}A$ mutant was shown to be transcriptionally more active than the wild type, which was taken as an indication that the mutant functionally resembled methylated STAT1 (see 1.4.3). However, these experiments with GST fusion proteins of STAT1 were performed in cells that expressed endogenous STAT1 (Mowen et al., 2001; Shuai et al., 1996). Given the nuclear translocation defect that we uncovered, we wanted to explore the transcriptional activity of this mutant in STAT1-deficient U3A cells (Müller et al., 1993). U3A cells were transfected with GST-STAT1 or GST-STAT1-$R^{31}A$ expression constructs and reporter gene activity after stimulation with IFNα was measured (see 2.2.12). The expression levels of the STAT1 variant proteins were similar (see Fig. 3.12), and wild

type GST-STAT1 reproducibly induced the reporter gene about 3-fold (Fig. 3.14, GST-WT). However, no gene induction was observed in repeated experiments with the $R^{31}A$ mutant (Fig. 3.14, GST-$R^{31}A$), as one might have expected from its nuclear translocation phenotype. In addition, we examined the gene induction of a GAS-containing reporter gene following stimulation with IFNγ. However, already the wild type STAT1 protein fused to GST showed an impaired response to IFNγ in transiently reconstituted U3A cell (data not shown). In any case, the GST-$R^{31}A$ mutant did not lead to a further enhancement of reporter gene activity, as was reported by Mowen and co-authors (2001). In summary, we observed that in cells where interference with endogenous STAT1 can be excluded, the mutation of Arg^{31} to alanine abolished the transcriptional activity of the STAT1 molecule.

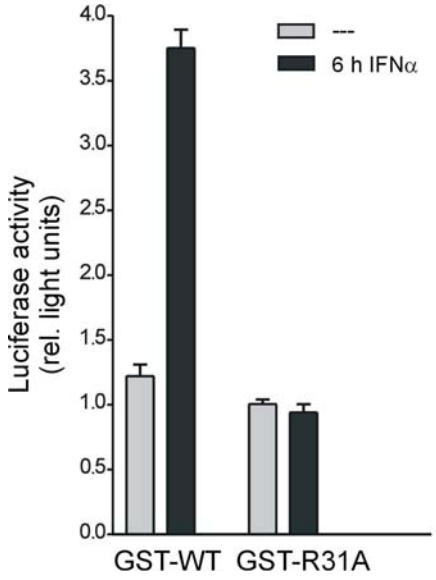

Fig. 3.14 Interferon α-induced reporter gene activity of wild type and $R^{31}A$ mutant STAT1-GFP fused to the C terminus of GST. STAT1-deficient U3A cells were transiently transfected with expression plasmids coding for N-terminal fusions of STAT1 with GST (GST-WT) or the respective $R^{31}A$ mutant (GST-$R^{31}A$). After 24 h the cells were stimulated with IFNα for 6 h or left untreated. Error bars represent standard deviations for six independent experiments.

3.1.8 Mass spectrometry and metabolic labelling both fail to provide evidence for the methylation of STAT1

The mutational analysis presented above demonstrated a crucial role for Arg^{31} in maintaining the structural integrity of the STAT1 N-domain. The mutation of arginine 31 to alanine caused instability of the N-domain, and the mutant failed to accumulate in the nucleus following cytokine stimulation, and to induce gene expression in STAT1-deficient cells (see

Figs. 3.8 and 3.14). These observations contradict that the $R^{31}A$ mutant protein is a valid model for arginine methylated STAT1 as suggested by Mowen et al. (2001). We therefore re-examined STAT1 arginine methylation and assessed its impact on IFN-induced transcription.

At first we employed mass spectrometry to investigate whether Arg^{31} is the acceptor of methyl group(s). Three independent analyses were performed, and the results were identical irrespective of IFN treatment of cells. U3A cells stably expressing Strep-tagged STAT1 were left untreated or stimulated with IFNα or -γ, before the cells were lysed and STAT1 was purified on a Strep-tactin resin. Subsequently, STAT1 resolved by denaturing SDS-PAGE was subjected to different mass spectrometric techniques (see 2.2.16 for details). Mass spectrometry was performed on STAT1 that was cleaved using the endoproteinase AspN and the resulting peptides were analysed with regard to the presence of methylated and/or non-methylated peptides which cover the position Arg^{31}.

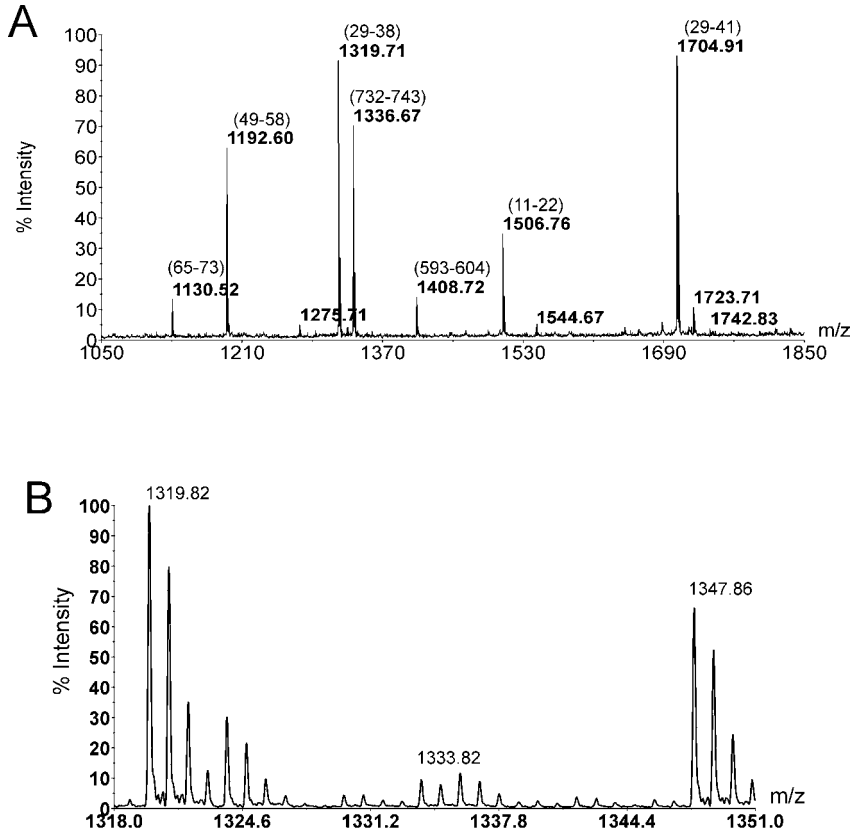

Fig. 3.15 MALDI mass analyses of STAT1 R^{31} methylation. (A) STAT1 was purified from U3A cells reconstituted with Strep-tagged STAT1. Peaks with *m/z* 1319.71 and 1704.91 correspond to the unmodified AspN fragments 29-38 and 29-41, respectively. (B) An equimolar mixture of synthetic peptides was used. Peaks with *m/z* 1319.8 and 1347.9 correspond to the unmodified and R^{31}-dimethylated AspN fragment 29-38, respectively.

Peptide mass fingerprint analyses done by MALDI-TOF measurements provided sequence coverage in the range of 60%. The MALDI mass spectra clearly revealed singly charged mass peaks at *m/z* 1319.71 and *m/z* 1704.91, corresponding to the unmodified STAT1 fragments ^{29}EIRQYLAQWL^{38} and ^{29}EIRQYLAQWLEKQ^{41} (one missed cleavage), respectively (Fig. 3.15A). Mass peaks which would match with Arg^{31}-methylated sequences (+14 mass units per methyl group) were definitely not present. The amino acid sequences of the unmodified peptides 29-38 and 29-41 were confirmed by nanoLC-ESI-MS/MS. Thus, collision-induced fragmentation of the unmodified peptide 29-41 (doubly charged precursor ion with *m/z* 852.94 in Fig. 3.16A) resulted in C-terminal y" fragment ions and a series of N-terminal b ions which clearly confirmed the presence of the non-methylated STAT1 peptide, as shown in Fig. 3.16B. NanoLC-ESI-MS analysis also revealed peaks with very low signal intensity which could match the methylated sequence 29-38. However, fragmentation by tandem MS undoubtedly showed that this signal is not attributed to the methylated STAT sequence (data not shown). Hence, the MS analyses show that exclusively unmodified peptides covering the position 31 of STAT1 could be detected. Considering that unmodified peptides were found with high peak intensities using two different MS methods, we concluded that STAT1 is not methylated at position Arg^{31} to a significant extent.

In addition, we synthesised R^{31} unmethylated (*m/z* 1319.8 and 1709.9) and R^{31} dimethylated (+ 28 mass units) peptides corresponding to the mentioned AspN fragments of STAT1. MALDI and ESI measurements (Figs. 3.15B and 3.16C) yielded comparable ion intensities irrespective of methylation, thus excluding the possibility that methylated peptides went undetected due to insufficient ionisation. Considering the optimal peak intensities and the excellent signal-to-noise ratio of our MS analyses with the native material, we concluded that STAT1 is not methylated at R^{31} to a significant extent.

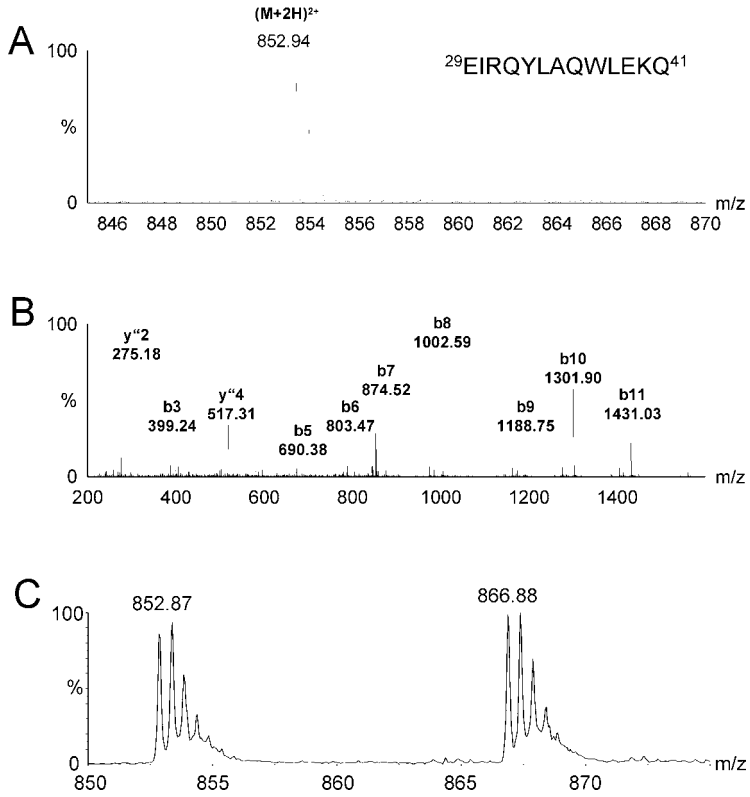

Fig. 3.16 Identification of unmodified R^{31} from native STAT1 and detection of R^{31}-methylated synthetic peptides. (A) ESI-MS spectrum of the unmodified peptide 29-41 separated by nanoLC (retention time 49.1 min). The peak with m/z 852.94 corresponds to the doubly charged ion of the unmodified sequence 29-41. (B) Fragment ions (MS/MS spectrum) resulting from the doubly charged precursor with *m/z* 852.94. Relevant ions were labelled according to the accepted nomenclature. Both the y ions and the b ions were produced by consecutive fragmentation reactions and confirmed the presence of the sequence 29-41 with an unmodified arginine at position 31. (C) ESI mass spectrum of an equimolar mixture of unmodified and R^{31}-dimethylated fragment 29-41 prepared by solid-phase peptide synthesis. Peaks with *m/z* 852.9 and 866.9 correspond to the doubly charged ions of the unmodified and dimethylated peptides, respectively.

Nevertheless, we used metabolic labelling of HeLa S3 cells as an unbiased approach to possibly identify other methylation sites in the STAT1 molecule (Fig. 3.17). Metabolic labelling of IFNα-treated HeLa cells by using L-[*methyl*-^{3}H]methionine was performed in the presence of translation inhibitors to examine whether STAT1 was methylated *in vivo*. The presence of translation inhibitors ensured that the labelling was due to post-translational methylation, not a low level of translational incorporation of L-[*methyl*-^{3}H]methionine in newly synthesised proteins (Liu and Dreyfuss, 1995). In two separate experiments STAT1 was immunoprecipitated from HeLa S3 cells that were metabolically labelled. Whole cell extracts and immunoprecipitated proteins were resolved by SDS-PAGE. Subsequent

fluorography revealed that several proteins were labelled in HeLa S3 cells, but that STAT1 was not (Fig. 3.17A). Silver staining (Fig. 3.17B) and immunoblotting (Fig. 3.17C) with anti-STAT1 antibodies confirmed that STAT1 was immunoprecipitated. Performing the metabolic labelling with L-[^{35}S]methionine in the presence of protein synthesis inhibitors demonstrated that virtually no label was incorporated under these conditions (Fig. 3.17D). These controls verified that the protein synthesis inhibitors were functioning properly and *in vivo* methylation had generally occurred. Nevertheless, no evidence for the methylation of STAT1 could be found.

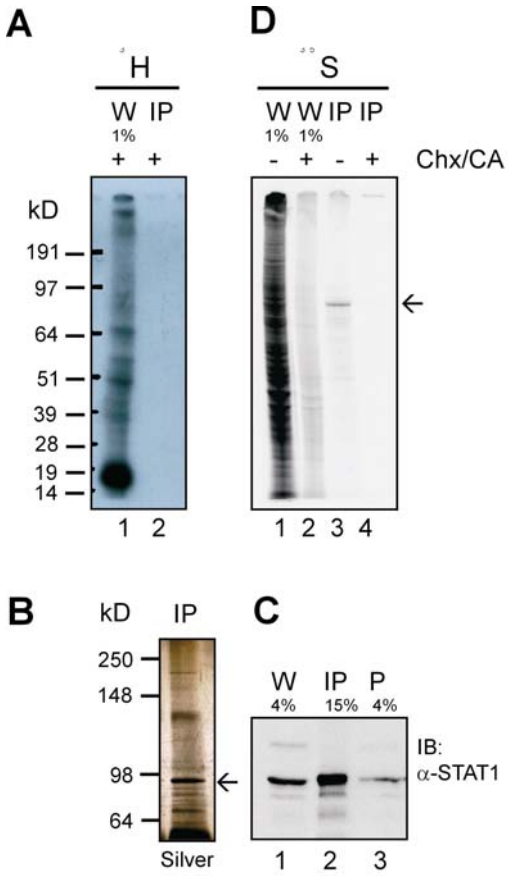

Fig. 3.17 Absence of *in vivo* methylation of STAT1. (A) HeLa cells were incubated with the methyl donor L-[*methyl*-^{3}H]methionine in the presence of protein synthesis inhibitors cycloheximide and chloramphenicol. Shown is the methylation pattern as determined by fluorography. The gel was loaded with 1% of the whole cell extract (W) or the immunoprecipitate obtained with a STAT1-specific antibody (IP). The exposure time was 2 weeks. (B) Silver staining of an immunoprecipitate as it was used in (A). (C) Immunoblot analysis with a STAT1 antibody of an immunoprecipitation reaction as performed in (A). The gel was loaded with 4% of the whole cell extract (lane 1), 15% of the immunoprecipitate (lane 2), and 4% of the post-IP supernatant (lane 3). (D) Incorporation of L-[^{35}S]methionine in nascent proteins in the absence (lanes 1 and 3) or presence (lanes 2 and 4) of protein synthesis inhibitors cycloheximide (Chx) and chloramphenicol (CA). Shown are phosphoimaging results with whole cell extracts (W; 1% was loaded) or the immunoprecipitate with a STAT1-specific antibody. The exposure time was 3 days. Arrows indicate the position of STAT1. Molecular weight markers are shown to the left (in kDa).

3.1.9 Methylthioadenosine affects gene transcription in an unspecific and STAT1-independent manner

A central argument in support of STAT1 arginine methylation was the observation that treatment of HeLa cells with the methyltransferase inhibitor methylthioadenosine (MTA, Fig. 3.20A) specifically inhibited IFNα-induced transcription (Mowen et al., 2001). Since we were unable to detect arginine methylation of STAT1 with two independent techniques (mass spectrometry and *in vivo* labelling), we decided to re-investigate the effect of MTA on interferon α-induced transcription. We measured the induction of a transiently transfected reporter gene by IFNα in the presence or absence of MTA (Fig. 3.18). DMSO or MTA (0.75 mM final) in DMSO was added to the cells three hours before stimulation with IFNα . In agreement with the previous report, we found that MTA reduced the IFNα-responsiveness of a luciferase reporter gene (Fig. 3.18).

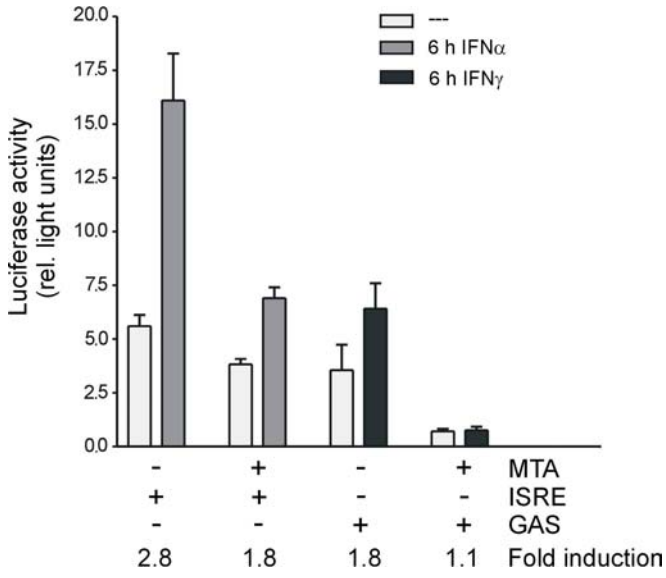

Fig. 3.18 Influence of MTA on cytokine-inducible gene expression. HeLa cells were co-transfected with interferon α or γ-responsive luciferase reporter genes and β-galactosidase expression constructs. After 24 h MTA (0.75 mM) or the same volume DMSO (0.75% final) was added and left on the cells for 3 h. Thereafter, the cells were incubated for another 6 h in the absence (white bars) or the additional presence of IFNα (grey bars) or IFNγ (black bars). Shown are the means of the normalised luciferase activities (arbitrary units) and the standard deviations for 6 independent experiments each. The respective numerical values for fold induction are given below the graph.

Next, we tested for the specificity of MTA by probing the response of HeLa S3 cells to IFNγ with a STAT1-dependent reporter gene and to tumor necrosis factor alpha (TNFα) with a NF-κB-dependent reporter. Clearly, signalling by both pathways was

diminished by MTA, as the respective luciferase reporter gene activities were drastically reduced (Figs. 3.18 and 3.19A). To exclude that these effects were caused by an adverse effect of MTA on the enzymatic luciferase activity rather than its mRNA expression, we performed RT-PCR analysis and confirmed the loss of luciferase gene induction after MTA treatment (Fig. 3.19B). Moreover, MTA did not interfere with the nuclear accumulation of NF-κB following TNFα treatment (Fig. 3.19C).

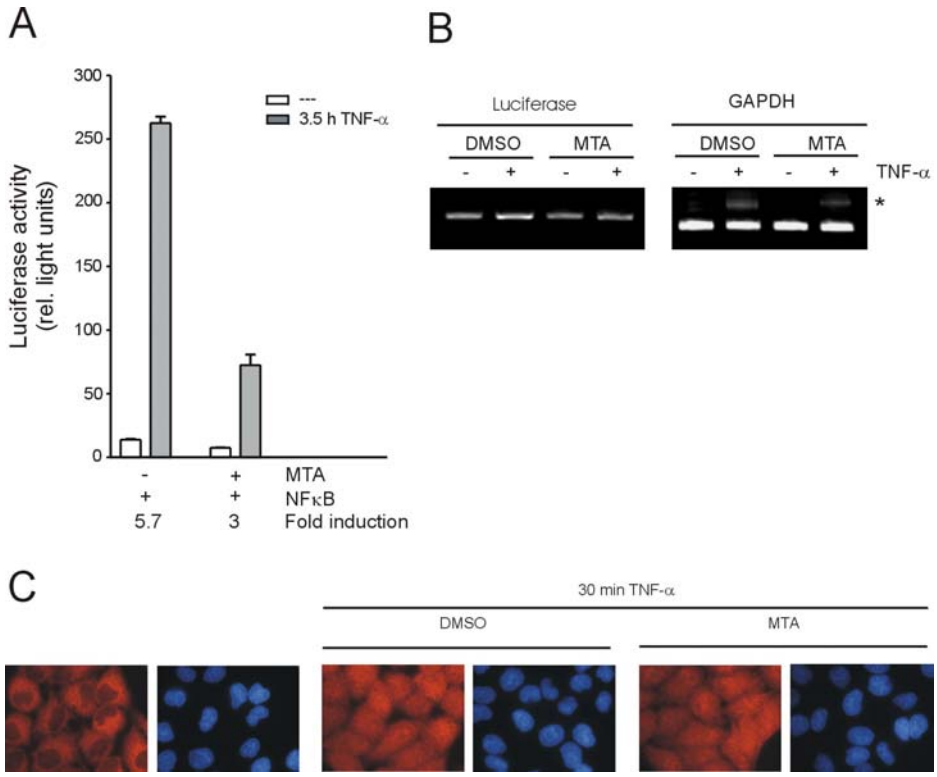

Fig. 3.19 Impact of MTA on TNFα-signalling. (A) Same as in Fig. 3.18, except that a luciferase reporter gene with multiple NF-κB binding sites was used. IFN was replaced by tumor necrosis factor α, which was left on the cells for 3.5 h. (B) RT-PCR analysis of luciferase expression from cells treated as in (A). The asterisk (*) denotes an unspecific PCR product. (C) Immunodetection of the p65 subunit of NF-κB in cells treated 30 min with TNFα. HelaS3 cells were either 3 h pretreated with MTA or the carrier DMSO. Following fixation with formaldehyde, cells were permeabilised for 15 min with 0.2% Triton X-100. For detection a Cy3-labelled secondary antibody was used (red). Hoechst staining is given in blue to highlight the nuclei.

To explore the possible cause of the unspecific effects of MTA on transcription, we examined the influence of MTA on tyrosine phosphorylation and dephosphorylation as well as on DNA binding of STAT1 in response to IFNα and IFNγ. Contrary to a previous report

(Mowen et al., 2001), MTA treatment strongly reduced the level of tyrosine phosphorylation of STAT1 (Fig. 3.20B). The negative influence of MTA on STAT1 tyrosine phosphorylation was confirmed in two different cell lines, HeLa S3 and MCF-7 cells (Fig. 3.21A), and was also reflected in the impaired nuclear accumulation of STAT1-GFP in transiently transfected HeLa S3 cells that were stimulated with either IFNα or IFNγ (Fig. 3.20C).

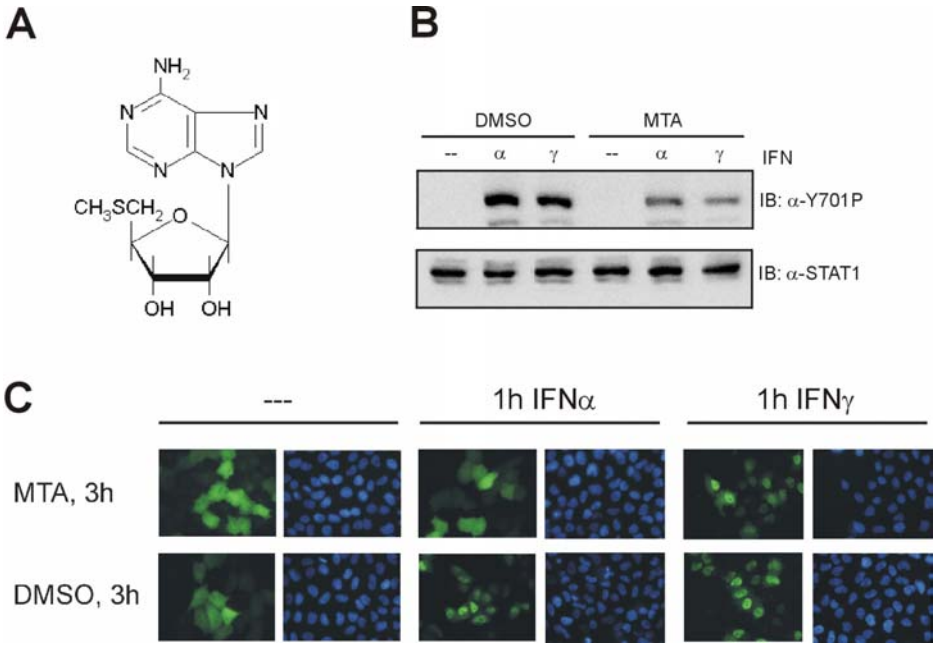

Fig. 3.20 Influence of the methyltransferase inhibitor MTA on STAT1 activation and nuclear accumulation. (A) Chemical structure of MTA (5'-deoxy-5'-methylthioadenosine). (B) MTA inhibits tyrosine phosphorylation of STAT1. MCF-7 cells were incubated for 3 h with medium containing carrier (DMSO) or MTA (0.3 mM). Subsequently, the cells were left untreated or stimulated with IFNα or -γ for 30 min as indicated. Shown are Western blot results of whole cell extracts with antibodies against tyrosine-phosphorylated STAT1 (α-Y701P) or total STAT1 (α-STAT1). (C) MTA interferes with the nuclear accumulation of STAT1. HeLa S3 cells transiently expressing STAT1-GFP were pretreated as in (B), and then stimulated for 1 h with the indicated interferon. Cells were fixed with formaldehyde and stained with Hoechst 33258 to indicate the nuclei (blue). The GFP signal is depicted in green.

We then tested the STAT1 DNA binding activity with a M67 probe, which is recognised by STAT1 homodimers. Gel shift analysis revealed that the DNA binding activity was correlated to the extent of tyrosine phosphorylation (Fig. 3.21 B). Thus, MTA treatment of cells did not generally inhibit DNA binding activity.

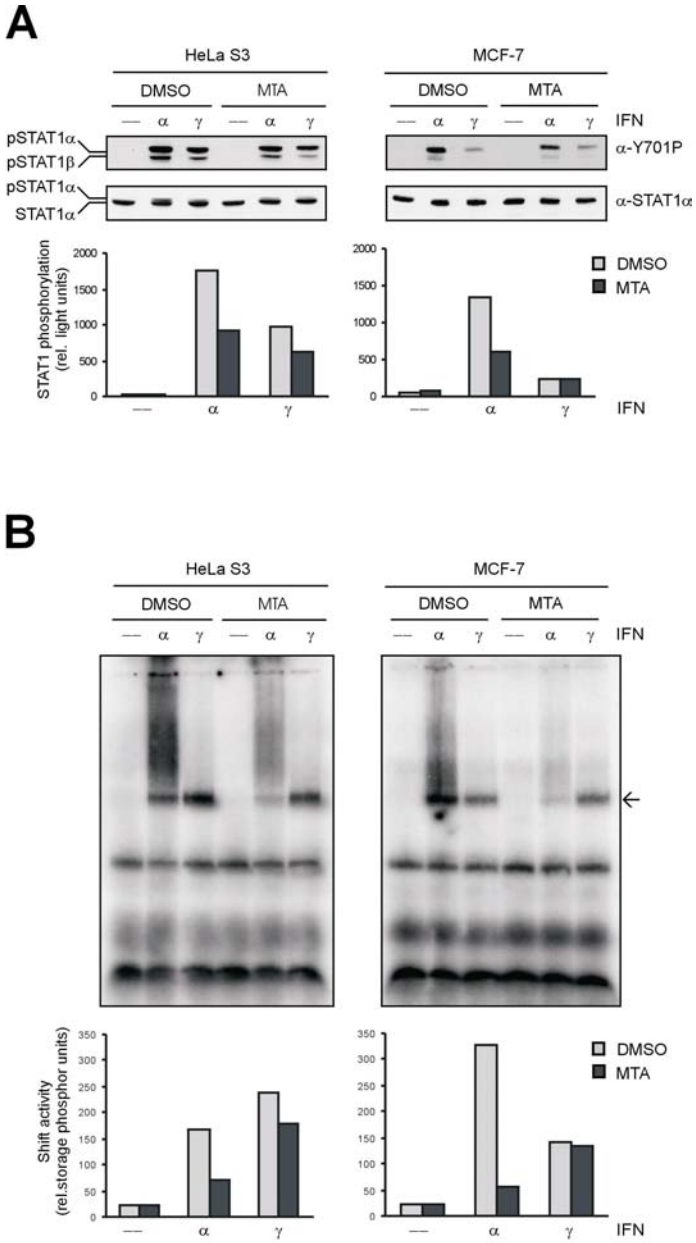

Fig. 3.21 MTA treatment of cells results in reduced activation of STAT1 and a corresponding decrease in DNA binding activity. (A) HeLa cells or MCF-7 cells were treated without or with MTA (0.75 mM) for 3 h. Subsequently, the cells were stimulated with IFNα or IFNγ for 60 min or left unstimulated. Shown are Western blot results with cytosolic cell extracts and a phosphotyrosine-specific STAT1 antibody (α-Y701P) as well as the reprobing with a STAT1 antibody (α-STAT1α). The migration of full length STAT1α and the C-terminal splice variant STAT1β is indicated. The Western blot signal intensities were analysed in a Lumi Imager (Roche) and depicted as a bar diagram. (B) Gel shift analysis of the extracts described in (A) using a M67 probe. The signal intensities were analysed with a phosphoimaging system (Storm) and depicted as a bar diagram. The arrow on the right margin of the gel marks the STAT DNA binding complex.

To test whether MTA exerted its effects on STAT1 tyrosine phosphorylation via the N-domain, we employed a STAT1 deletion mutant that lacked residues 1-126 (ΔN). As is

shown in Fig. 3.22, MTA reduced the tyrosine phosphorylation of both the wild type and the truncated STAT1. These results ruled out that modification of arginine 31 was responsible for the observed effects.

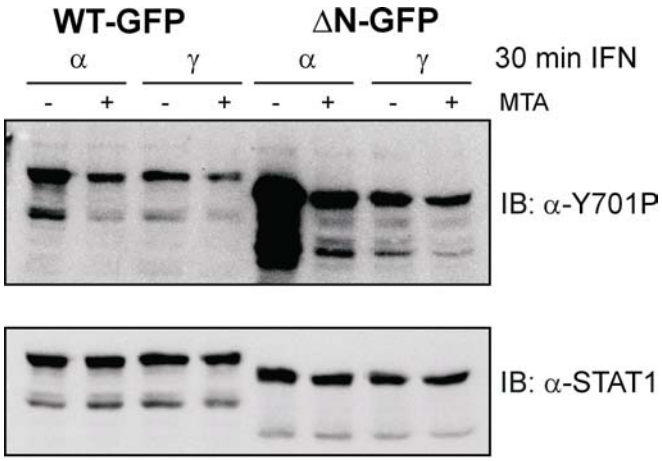

Fig. 3.22 MTA inhibits STAT1 phosphorylation even in the absence of the N-domain. U3A cells expressing full length STAT1 (WT-GFP) or the N-terminal deletion mutant lacking residues 1-126 (ΔN-GFP), both fused to the green fluorescent protein, were incubated for 3 h with medium containing MTA (0.75 mM) or carrier (DMSO). Subsequently, IFNγ or -α was added for 30 min, before whole cell extracts were prepared. Shown are Western blot results with antibodies directed against tyrosine-phosphorylated STAT1 (α-Y701P), and the reprobing with a STAT1-specific antibody (α-STAT1).

Moreover, also phosphatase activities were diminished, as the phosphorylated STAT1 resisted dephosphorylation better in the MTA-treated cells than in control cells (Fig. 3.23, WT-GFP). To analyse the dephosphorylation of STAT1, transiently reconstituted U3A cells were stimulated for 30 min with IFNα. Subsequently, the cells were treated with the kinase inhibitor staurosporine, to block re-phosphorylation. As can be seen in Fig. 3.23, MTA again decreased the level of STAT1 tyrosine phosphorylation (compare lanes 2 and 6). However, in the presence of MTA, the level of tyrosine phosphorylation remained nearly constant over a time of 90 min, indicating an impaired dephosphorylation (Fig. 3.23, compare lanes 6-9 to lanes 2-5). This phenomenon was noted before also by others and explained by the reduced affinity of non-methylated STAT1 to the phosphatase TC45 (Zhu et al., 2002). We observed a similar dephosphorylation defect, in the presence of MTA, with the N-terminal deletion mutant of STAT1 (Fig. 3.23, ΔN-GFP, lanes 15-18). Yet, again, the overall level of STAT1 tyrosine phosphorylation was drastically reduced in MTA-treated cells, even in the absence of

the N-domain, arguing against a role of methylation in phosphatase recruitment (Fig. 3.23, compare lanes 11-14 to lanes 15 to 18).

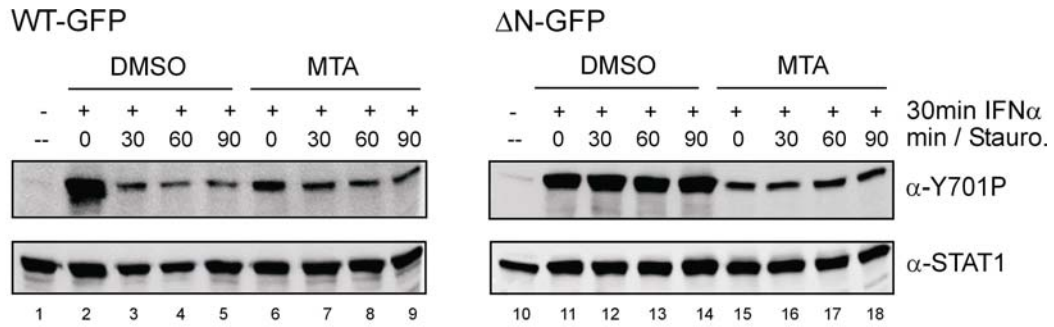

Fig. 3.23 MTA treatment of cells modulates both STAT1 tyrosine phosphorylation and dephosphorylation. U3A cells expressing full length STAT1 (WT-GFP) or the N-terminal deletion mutant (ΔN-GFP) were incubated for 3 h with medium containing MTA (0.75 mM) or carrier (DMSO). Following a 30 min IFNα treatment, the kinase inhibitor staurosporine was added for the indicated times, before whole cell extracts were prepared. STAT1 activation was monitored in a Western blot analysis with antibodies directed against tyrosine-phosphorylated STAT1 (α-Y701P), and the reprobing with a STAT1-specific antibody (α-STAT1).

Importantly, reduced dephosphorylation was also observed in a STAT1 unrelated pathway. In the presence of MTA, the transient TNFα-induced serine phosphorylation of the MAP kinase p38 was drastically prolonged (Fig. 3.24). In conclusion, we note that methylthioadenosine influenced multiple signalling pathways and different enzymatic reactions in an unspecific manner.

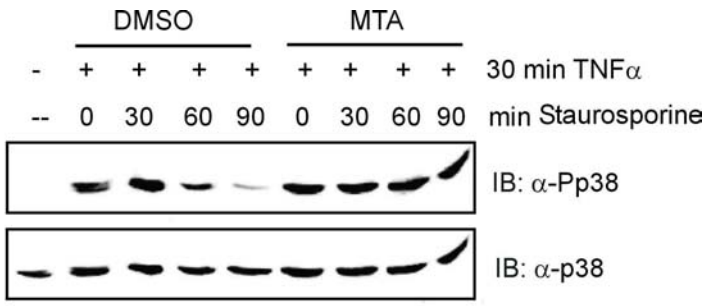

Fig. 3.24 Dephosphorylation of p38 is blocked in the presence of MTA. HeLa S3 cells were preincubated without or with 0.75 mM MTA for 3 h following a 30 min stimulation with TNF-α (20 ng/ml). To block continued phosphorylation, the kinase inhibitor staurosporine was added for the indicated times after stimulation. Shown is a Western blot analysis with whole cell lysates using a phospho-p38 antibody. Subsequently, the blot was stripped off the antibody and reprobed with a p38-specific antibody.

3.1.10 MTAP expression does not improve the interferon response of MCF-7 cells

Numerous cancer cells are defective in the expression of 5'-deoxy-5'-methylthioadenosine phosphorylase (MTAP) (Kamatani et al., 1982; Fitchen et al., 1986; Nobori et al., 1996; Garcia-Castellano et al., 2002), an enzyme which among other reactions can catalyse the efficient breakdown of the methyltransferase inhibitor MTA (Kamatani et al., 1981). Mowen and colleagues (2001) reasoned that the interferon insensitivity of certain tumor cell lines might be causally linked to MTAP deficiency, since MTA is also endogenously produced as a metabolic intermediate in the catabolism of bioactive amides (Williams-Ashman et al., 1982),. According to their model, reconstitution of MTAP-deficient cells with the functional enzyme should decrease the level of endogenous MTA, and ultimately restore the response of the tumor cells to interferons. To test this hypothesis, we reconstituted human breast cancer MCF-7 cells, which carry a homozygous deletion of exons 5-8 of MTAP (Nobori et al., 1996), with an MTAP expression clone and evaluated the IFN response in a transient luciferase reporter gene assay (Fig 3.25).

First, the MTAP deficiency of these cells was confirmed by RT-PCR analysis with a primer pair binding to the boundary of exon 1 and 2 and to exon 6, respectively. The expected PCR product of 521 base pairs was observed in transiently reconstituted MCF-7 cells and HeLa S3 control cells, but was absent from native MCF-7 cells (Fig. 3.25A). MCF-7 cells were transiently co-transfected with the MTAP expression clone or empty vector and an IFNα-responsive ISRE- or an IFNγ-responsive GAS-containing luciferase reporter gene. MTAP was expressed as a GFP fusion protein, and its presence did not influence tyrosine phosphorylation of STAT1 after interferon stimulation of cells (Fig. 3.25B). Twenty-four hours after transfection with either GFP-MTAP or with GFP, the MCF-7 cells were incubated with IFNα or -γ for 6 h before luciferase activity was determined in cell extracts. As is shown in Fig. 3.25C, MCF-7 cells responded to IFNα with an about 8-fold induction, and to IFNγ with an about 24-fold induction of the reporter gene. However, the expression of MTAP in these cells did not increase the transcriptional yield (Fig. 3.25C, D).

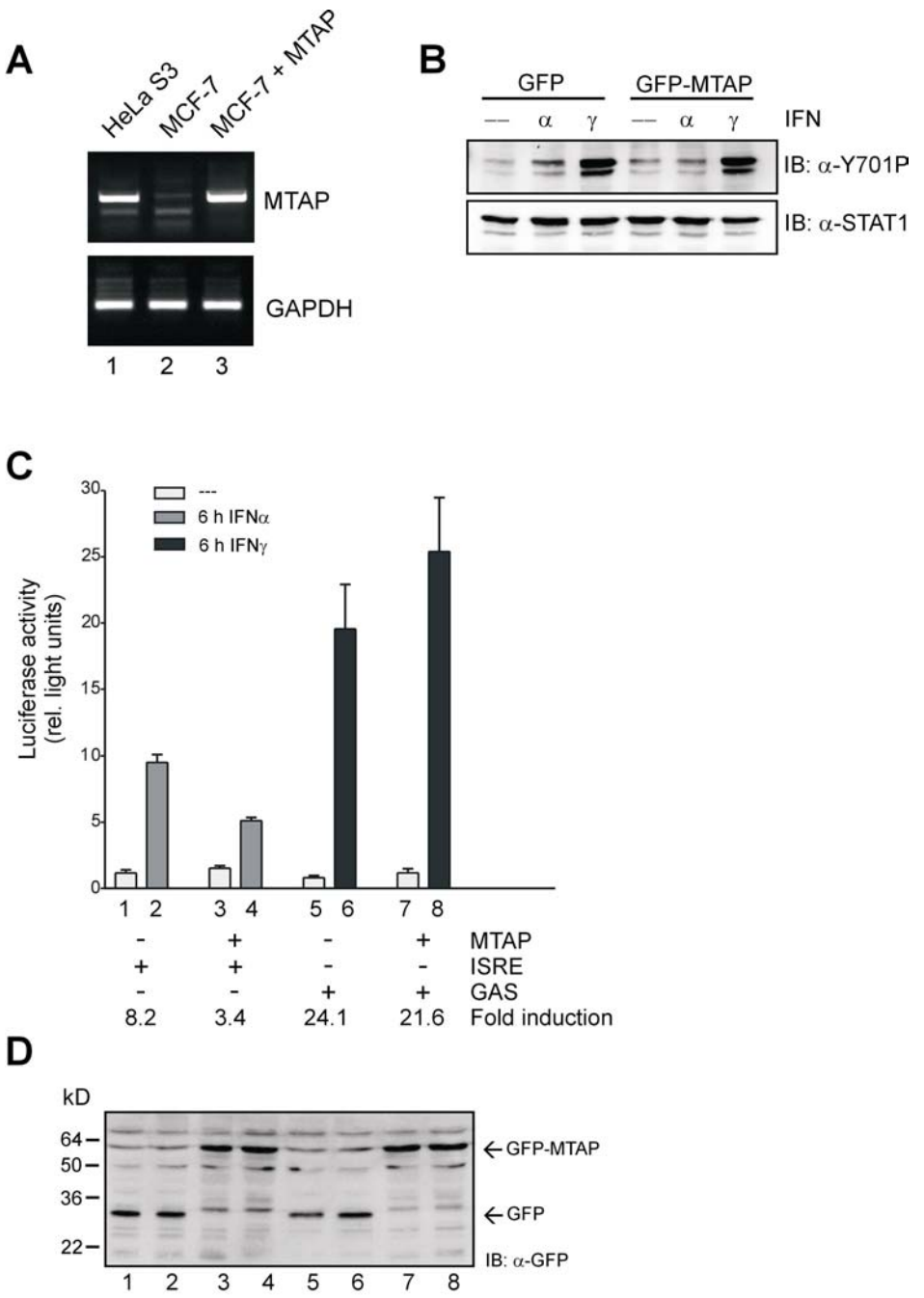

Fig. 3.25 Influence of MTAP expression on IFN-induced reporter gene activity. (A) RT-PCR analyses with primers specific for GAPDH or MTAP. MCF-7 cells were transfected with empty vector pEGFP-C2 (lane 2) or this vector containing MTAP cDNA (lane 3). RT-PCR was performed after 72 h. As a control, untreated HeLa cells were used (lane 1). (B) Western blot results of whole cell extracts from transiently reconstituted MCF-7 cells, probed with a phosphotyrosine-specific STAT1 antibody (α-Y701P, top). Subsequently, the blot was reprobed with a STAT1-specific antibody (α-STAT1, bottom). MTAP-deficient MCF-7 cells were transfected with pEGFP-C2 or this vector containing MTAP cDNA as indicated. After 30 h the cells were stimulated without or with interferon α or -γ for 60 min before extracts were prepared. (C) Reporter gene induction in MTAP-deficient MCF-7 cells that had been co-transfected with either IFNα- or IFNγ-responsive luciferase reporter genes (containing

multiple ISRE or GAS elements in their promoters, respectively), β-galactosidase expression plasmid, as well as with vectors expressing GFP or GFP-MTAP as indicated. Twenty-four hours after transfection, the cells were treated for 6 h without (white bars) or with IFNα (grey bars) and IFNγ (black bars), respectively. Shown are the means of the normalised luciferase activities (arbitrary units) and the standard deviations for 6 independent experiments each. The respective numerical values for fold induction are given below the graph. (D) Western blot results with whole cell extracts derived from the cells used in (C). The blot was probed with an antibody directed against GFP.

3.2 Characterisation of ratjadone A – a new inhibitor of CRM1-mediated nuclear protein export

3.2.1 Ratjadone A inhibits CRM1-mediated nuclear protein export

Ratjadone A was proposed to inhibit nuclear protein export, due to its similar structure and similar cytotoxic effects to the known nuclear export inhibitor leptomycin B (LMB, see 1.5). In order to test whether ratjadone A indeed acts as an nuclear export inhibitor we analysed its impact on nuclear protein export in two different assays in comparison to LMB. At first, we examined if ratjadone A can revert the cytoplasmic accumulation of a protein that contains a canonical nuclear export signal (NES, see 1.5). A reporter protein consisting of GFP fused to a canonical NES, amino acids 365-427 of human STAT1 (Meyer et al., 2002a), was expressed in mammalian cells. The steady state localisation of this protein is cytoplasmic, contrary to GFP with a pancellular or predominantly nuclear localisation (compare Fig. 3.27A and D). Due to their small size (<30 kDa), these proteins are capable of passing through the nuclear pore by free diffusion (Paine and Feldherr, 1972). Treatment of cells expressing GFP for 60 min with 10 ng/ml LMB or 10 ng/ml ratjadone A was without detectable influence on the subcellular distribution of GFP (Fig. 3.27E, F). Contrary, the same treatment abolished the cytoplasmic accumulation of GFP-NES, which was now found in both the nucleus and the cytoplasm (Fig. 3.27B, C).

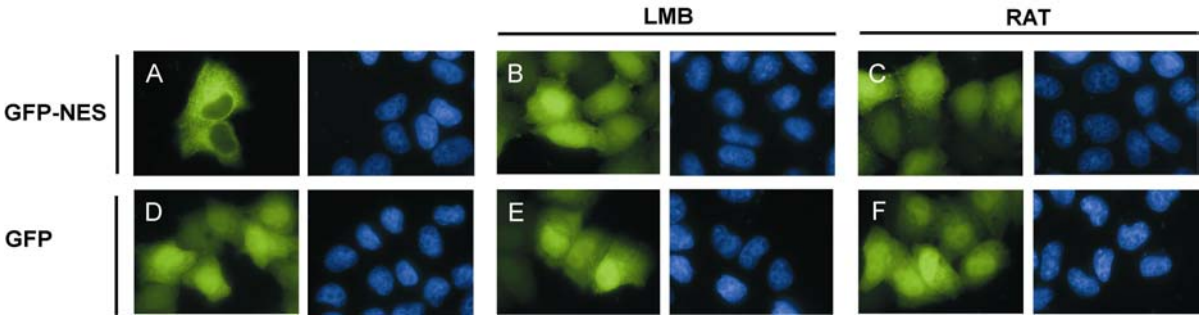

Fig. 3.27 Ratjadone A causes nuclear accumulation of a NES-containing reporter protein. HeLa S3 cells were transiently transfected with pGFP-NES (A-C) or with a GFP expression vector (D-F). Twenty-four hours after transfection cells, were treated with LMB (B, E) or ratjadone A (C, F) for 1 h or left untreated (A, D). Subsequently, cells were fixed with formaldehyde and stained with Hoechst 33258 to indicate the nuclei (blue). The GFP signal is depicted in green.

Next, a microinjection assay was used to specifically reveal the inhibitory effect of LMB and ratjadone A on nuclear export. Here, a recombinant reporter protein consisting of a fusion of GST and GFP was purified from bacteria and subsequently injected into the nucleus of HeLa cells. Its large size (55 kDa) precluded free diffusion across the nuclear envelope (Fig. 3.28A). The insertion of cDNA coding for a STAT1 NES activity (aa 365-427) between the genes coding for GST and GFP resulted in a bacterial expression construct that yielded the export reporter protein GST-NES-GFP. As is shown in Fig. 3.28B, a one hour incubation period following nuclear microinjection of the export reporter resulted in its steady state cytoplasmic accumulation. Preincubation of the cells with ratjadone A or LMB for 3 h before microinjection completely blocked the subsequent nuclear export of the NES fusion protein (Fig. 3.28C, D). These results confirm the previous observation that both bacterial metabolites inhibit the nuclear export of NES-containing proteins at a similar concentration (Köster et al., 2003).

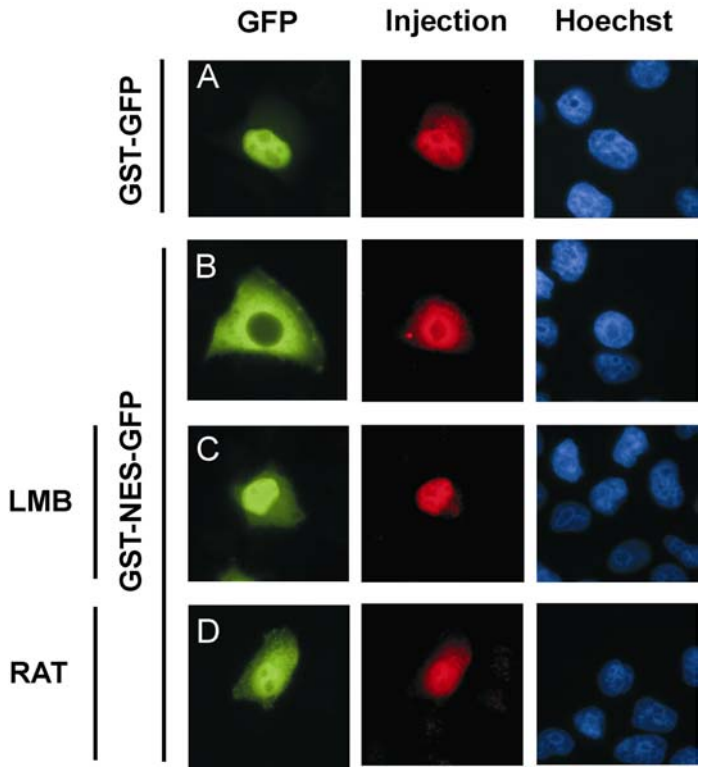

Fig. 3.28 Ratjadone A blocks the nuclear export of a reporter protein containing a canonical NES. The indicated GST-GFP fusion proteins were injected into the nuclei of HeLa S3 cells. One hour after microinjection cells were fixed and stained with Hoechst 33258 to show the nuclei (blue). The site of injection is given by the co-injected marker protein TRITC-BSA (red). The GFP signal is shown in green. In C and D cells were preincubated with the indicated export inhibitor for 3 h before microinjection.

A major unanswered question concerns the reaction mechanisms of ratjadones and LMB, both of which target CRM1. The molecular mechanism of CRM1 inactivation was identified as the covalent addition of LMB through its α,β-unsaturated δ-lactone to the sulfhydryl group of residue Cys^{528}. To investigate whether Cys^{528} was targeted also by ratjadones, which similar to LMB contain an unsaturated lactone (Fig. 1.6), we followed a procedure that was employed by Kudo et al. (1999) to demonstrate the modification by LMB of Cys^{528} of human CRM1. An 18mer peptide (residues 513-530), additionally comprising the stretch of conserved hydrophobic amino acids in the N-terminal flanking region of Cys^{528} (residues 517-528), was synthesised and reacted without or with ratjadone A. Mass spectrometric analysis of the unreacted material revealed a mass peak of the unmodified CRM1 peptide at m/z 2103.06. After the incubation with ratjadone A an additional peak at m/z 2559.40 was detected, which corresponds to the adduct of the peptide and ratjadone A (Fig. 3.29). The amino acid sequence and the site of ratjadone modification was confirmed by tandem MS. The evidence for the alkylation of Cys^{528} comes from the presence of unmodified N-terminal b ions and the neutral loss of the ratjadone moiety during fragmentation (data not shown).

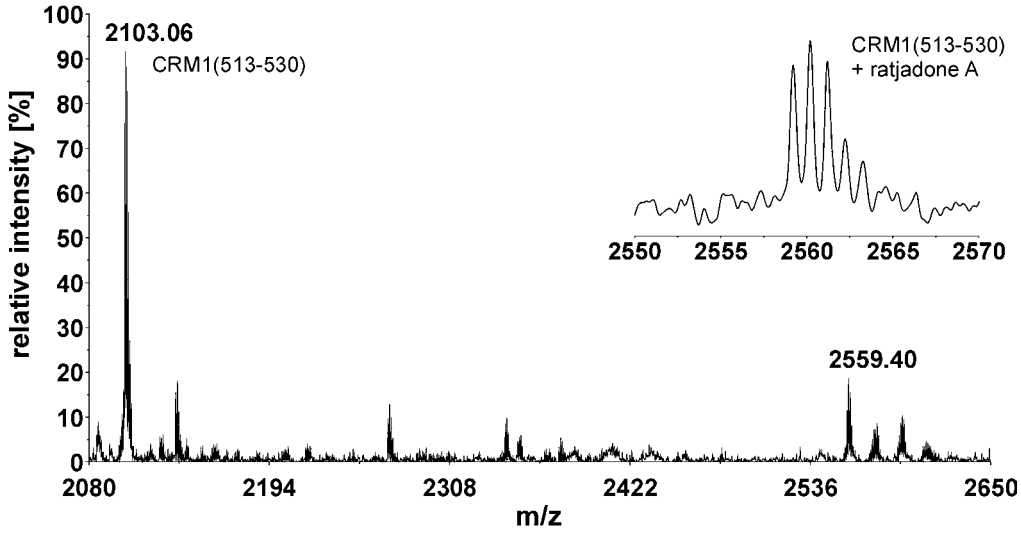

Fig. 3.29 Ratjadone A covalently binds to Cys^{528} of a CRM1-peptide. Synthetic human CRM1 (residues 513–530) that contains Cys^{528} was incubated with ratjadone A for 24 h at 37°C and analysed by MALDI–TOF-MS. The peaks with m/z 2103.06 (theoretical m/z 2103.19) and 2559.40 (theoretical m/z 2559.48; see also enlargement) correspond, respectively, to the unmodified and ratjadone A-alkylated hCRM1 sequence ^{513}EKRFLVTVIKDLLGLCEQ^{530}.

We next analysed a mutant of human CRM1 with a serine mutation in position 528. Cysteine 528 is conserved between *S. pombe* and humans, which are LMB-sensitive, but not in LMB-insensitive organisms such as *Sac. cerevisiae*. Moreover, replacement of the Cys^{528} by serine resulted in insensitivity of *S. pombe* CRM1 towards LMB (Kudo et al., 1998; 1999). For our experiments, Flag-tagged expression constructs of wild type or mutant human CRM1 were co-expressed with GFP-NES in HeLa cells. As was described before for NIH3T3 cells (Kudo et al., 1997), CRM1 was localised mainly intranuclear or at the nuclear rim. Strongly overexpressing cells displayed also cytoplasmic staining. In this respect, no differences were observed between mutant and wild type CRM1 (Fig. 3.30 and data not shown). Moreover, the localisation of CRM1 was not sensitive towards LMB or ratjadone (Fig. 3.30). Contrary, treatment of cells with either LMB or ratjadone A precluded the cytoplasmic accumulation of GFP-NES in cells expressing wild type CRM1 (Fig. 3.30A), and a pancellular distribution of the reporter protein resulted (Fig. 3.30C, E). Expectedly, expression of the Ser^{528} mutant of CRM1 rendered cells insensitive to the activity of LMB, since the cytoplasmic accumulation of the NES-containing reporter persisted (Fig. 3.30D). Importantly, the identical phenotype was observed also after treatment with ratjadone A in the cells expressing the mutant CRM1 (Fig. 3.30F).

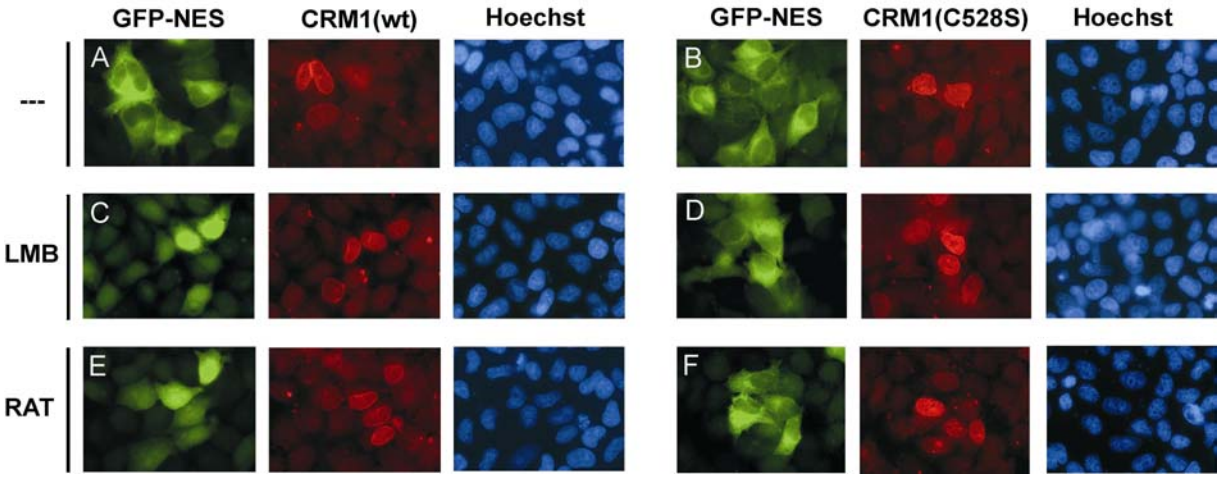

Fig. 3.30 Mutation of cysteine 528 to serine renders CRM1 resistant to both LMB and ratjadone A. HeLa S3 cells were cotransfected with GFP-NES and either wild type CRM1 (A, C, E) or the mutant CRM1($C^{528}S$) (B, D, F). Twenty-four hours later the cells were treated with ratjadone A or LMB (10 ng/ml each) for 3 h before fixation with formaldehyde. FLAG-tagged CRM1 was detected using a mouse monoclonal anti-FLAG antibody. The distribution of GFP-NES and the positions of Hoechst-stained nuclei are shown.

Thus, we concluded that both LMB and ratjadone A inhibit protein transportation *in vivo* by targeting residue Cys^{528} of CRM1. Given their identical and highly specific modes of molecular action, we propose that ratjadone A and LMB can be used interchangeably in the study of protein export from the nucleus.

3.2.2 Use of ratjadone A to study protein nuclear export

To proof the feasibility of ratjadone A as a tool in the study of protein nuclear export, we extended our analysis to known cellular substrates of CRM1-dependent export. The cytoplasmic redistribution of STAT1 following cytokine stimulation has been shown to be LMB-sensitive, indicating a contribution of CRM1-mediated export (Begitt et al., 2000; McBride et al., 2000). To test if ratjadone A treatment results in a similar export block, NIH 3T3 cells were transiently transfected with STAT1-GFP. The cells were pulse treated with IFNγ for 30 min and the redistribution of STAT1-GFP was monitored either in the presence or absence of ratjadone A (Fig. 3.31).

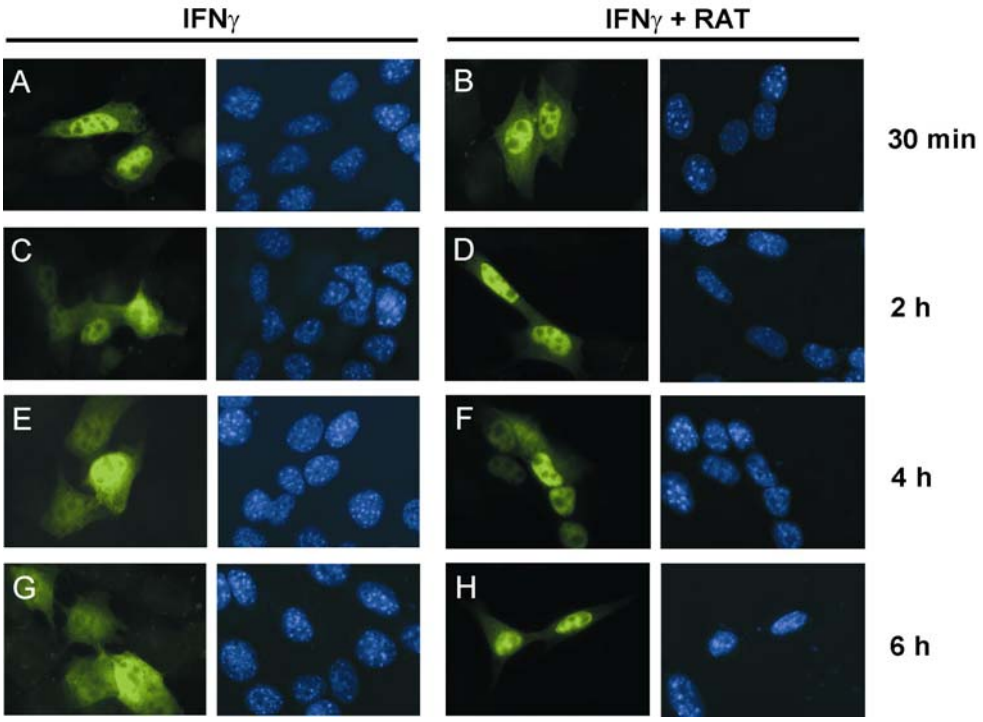

Fig. 3.31 Ratjadone A blocks the cytoplasmic redistribution of STAT1 after IFN stimulation. NIH 3T3 cells were transiently transfected with pSTAT1-GFP (A-H). Twenty-four hours after transfection cells were preincubated with cyclohexemide to inhibit protein synthesis. Subsequently, the cells were stimulated with IFNγ either in the presence of ratjadone A (B, D, F, H) for the indicated time or without addition of the export inhibitor (A, C, E, G). Shown is the distribution of STAT1-GFP (green) and the position of the nuclei stained with Hoechst 33258 (blue).

As can be seen in Fig. 3.31B, ratjadone A did not interfere with the nuclear accumulation of STAT1 following cytokine treatment. However, the relocalisation of STAT1 from the nucleus to the cytoplasm was drastically impaired in cells that were incubated with ratjadone A. Even 6 h following IFNγ stimulation STAT1-GFP showed persistent accumulation in the nucleus, when treated with ratjadone A (Fig. 3.31H). STAT1-GFP in the control cells had at the same time already almost completely relocalised to the cytoplasm (Fig. 3.31G).

Another well known CRM1-dependent export substrate is the p65 subunit of NFκ-B. As a shuttling protein, p65 rapidly accumulates in the nucleus of 3T3 cells upon LMB treatment (Birbach et al., 2002). However, the binding of NF-κB to CRM1 is not direct. The nuclear export signal is provided by the inhibitor of NF-κB (IκB) which binds to p65 in the nucleus and thereby directs its nuclear export (Johnson et al., 1999; Huang et al., 2000). As can be seen in Fig. 3.32A, overexpression of p65-GFP in HeLa S3 cells resulted in a heterogeneous cellular distribution. In the majority of the cells the GFP signal was detected in the cytoplasm only, however, about one third of the cells showed a pancellular distribution throughout both the cytoplasmic as well as the nuclear compartments, and in some cells even a nuclear accumulation was observed. Inactivation of CRM1 changed this distribution. In the presence of ratjadone A nearly all cells showed a homogenous, predominantly nuclear localisation of p65-GFP (Fig. 3.32B). As a control to indicate the CRM1 activity, GFP-NES was expressed in a parallel set of experiment. Expectedly, the cytoplasmic accumulation of the export reporter (Fig. 3.32C) was blocked in the presence of ratjadone A, and a pancellular distribution was observed (Fig. 3.32 D).

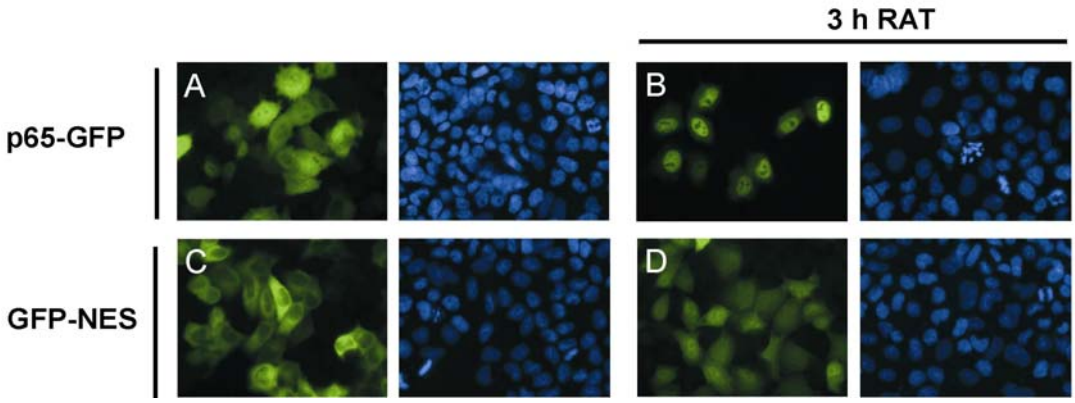

Fig. 3.32 Ratjadone A causes nuclear accumulation of a p65-GFP fusion protein. HeLa S3 cells were transiently transfected with p65-GFP (A, B) or with a pGFP-NES (C, D). Twenty-four hours after transfection cells were treated with ratjadone A (RAT; B, D) for 3 h or left untreated (A, C). Subsequently, cells were fixed with formaldehyde and stained with Hoechst 33258 (blue). The GFP signal is depicted in green.

3.2.3 CRM1-mediated export contributes to the nucleocytoplasmic distribution of STATs in resting cells

For more than a decade STATs were regarded as so-called 'latent' cytoplasmic transcription factors (Darnell, 1997). It was believed that STATs were gaining access to the nuclear compartment only following cytokine treatment to fulfil their function as transcription factors. In the meantime, however, more and more evidence accumulated that this static view of the JAK-STAT pathway had to be revised. We and other groups reported that STATs are found also in the nucleus of unstimulated cells (Chatterjee-Kishore et al., 2000; Meyer et al., 2002b), and it was observed that STATs can regulate the expression of certain genes in a phosphorylation-independent way (Kumar et al., 1997; Ramana et al., 2000; Meyer et al., 2002a; Ramana et al., 2002). Yet, the mechanism how STATs enter and exit the nucleus in the absence of a cytokine signal was not resolved.

During the course of this work we noticed that the export inhibitors ratjadone A and leptomycin B changed the nucleocytoplasmic distribution of STAT1 in resting cells. Following a 5 hour incubation with LMB the predominantly cytoplasmic localisation of STAT1-GFP gave way to an even, pancellular distribution (Fig. 3.33 B). Prolonged treatment did, however, not result in a nuclear accumulation, rather STAT1 was found in both compartments with the same intensities, indicating a diffusion-controlled equilibrium.

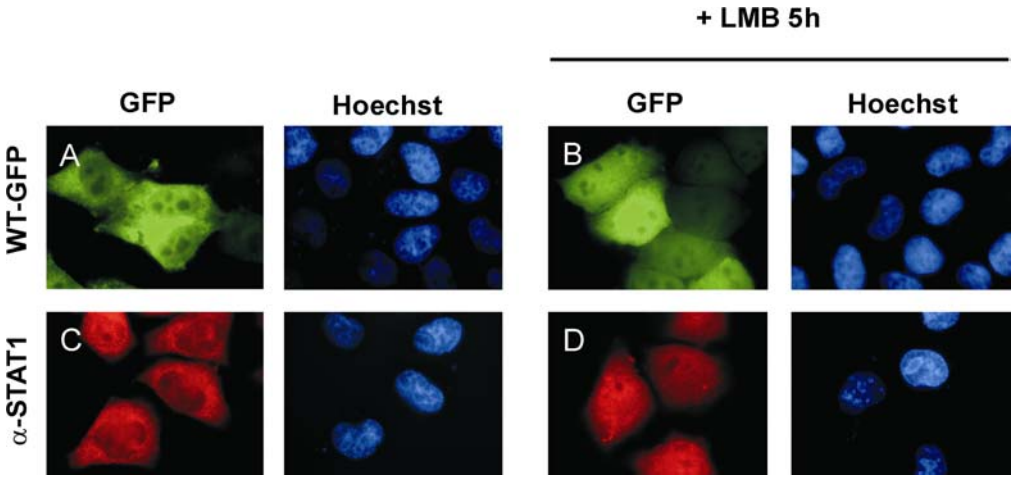

Fig. 3.33 Blocking CRM1 activity results in a nucleocytoplasmic redistribution of STAT1 in resting cells. HeLa S3 cells were transiently transfected with pSTAT1-GFP (A, B) or stained with an α-STAT1 antibody to highlight the cellular distribution of endogenous STAT1 protein (C, D). Twenty-four hours after transfection, cells were treated with ratjadone A (RAT; B, D) for 5 h or left untreated (A, C). The distribution of STAT1 fusion protein (WT-GFP) in formaldehyde-fixed cells is depicted in green. The positions of Hoechst-stained nuclei (blue) are shown. The antibody staining is given in red.

To rule out that free GFP may influence the result, the distribution of STAT1-GFP in HeLa S3 cells was compared to that of endogenous STAT1 visualised in an antibody staining (Fig. 3.33C, D). The same pancellular distribution was observed for endogenous STAT1 in HeLa S3 cells following a 5 hour incubation with leptomyin B (Fig. 3.33D). These results implicate CRM1-mediated export in controlling the nucleocytoplasmic distribution of STATs in resting cells. The LMB induced nuclear enrichment was not dependent on phosphorylation, since the same results were obtained with the tyrosine mutant STAT1 ($Y^{701}F$, data not shown), which cannot be phosphorylated. Equivalent results were obtained with the export inhibitor ratjadone A, and also in different cell lines (3T3 cells, Fig. 3.34 and data not shown).

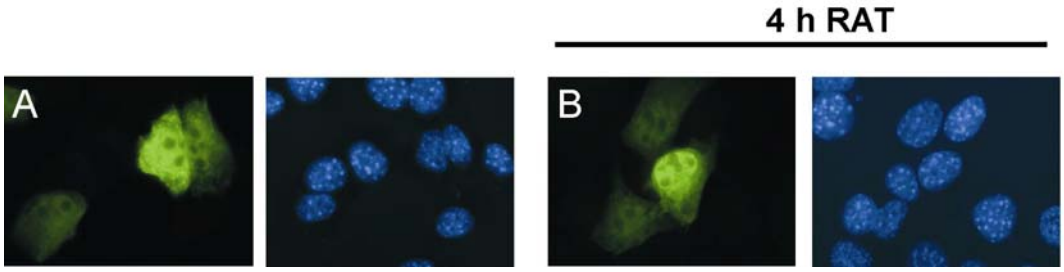

Fig. 3.34 Ratjadone A treatment results in nuclear accumulation of STAT1 in NIH 3T3 cells. Twenty-four hours after transfection with pSTAT1-GFP cells were treated with ratjadone A (B) for 4 h or left untreated (A). The GFP fluorescence (green) was evaluated in fixed cells that were counterstained with Hoechst 33258 (blue).

STAT3 was chosen as another STAT family member, and expressed as a GFP fusion protein in HeLa S3 cells. The nucleocytoplasmic distribution of GFP-STAT3 in resting cells is more nuclear than that of STAT1-GFP (compare Figs. 3.33A and 3.35A). As can be seen in Fig. 3.35B, a 3 hour incubation of HeLa S3 cells expressing GFP-STAT3 with ratjadone A led to a further nuclear enrichment that almost resembled nuclear accumulation following cytokine treatment. The results shown here for ratjadone A are identical to the observations of Bhattacharya and Schindler (2003) obtained with LMB, further indicating that LMB and ratjadone A can be used interchangeably in the study of nuclear protein export.

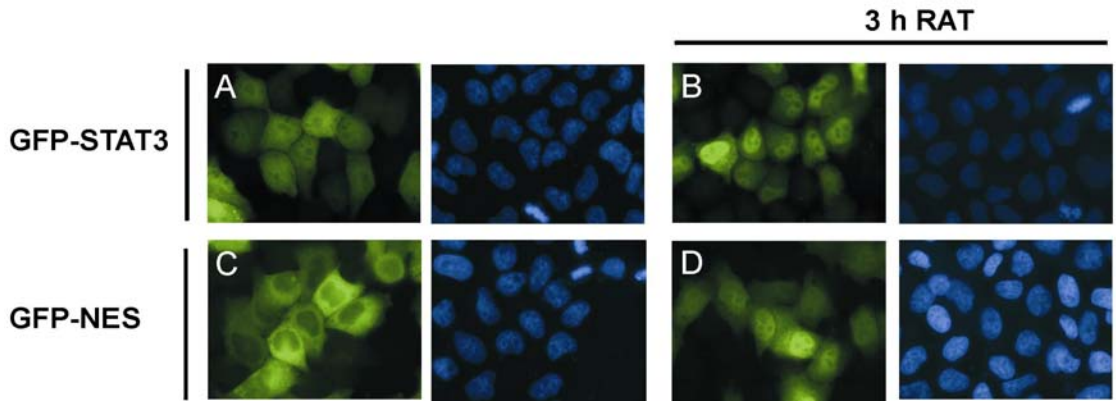

Fig. 3.35 STAT3 accumulates in the nucleus upon ratjadone A treatment. HeLa S3 cells were transiently transfected with GFP-STAT3 (A, B) or with a pGFP-NES (C, D). Twenty-four hours after transfection cells were treated with ratjadone A (B, D) for 3 h or left untreated (A, C). Subsequently, cells were fixed with formaldehyde and stained with Hoechst 33258 to indicate the nuclei (blue). The GFP signal is depicted in green.